HHS Public Access

Author manuscript

*Cell Rep*. Author manuscript; available in PMC 2023 October 23.

Published in final edited form as:

*Cell Rep*. 2023 August 29; 42(8): 112830. doi:10.1016/j.celrep.2023.112830.

# Premature aging and reduced cancer incidence associated with near-complete body-wide *Myc* inactivation

**Huabo Wang**[1], **Jie Lu**[1], **Taylor Stevens**[1], **Alexander Roberts**[1], **Jordan Mandel**[1], **Raghunandan Avula**[1,2], **Bingwei Ma**[3], **Yijen Wu**[4], **Jinglin Wang**[1,5], **Clinton Van't Land**[6], **Toren Finkel**[7], **Jerry E. Vockley**[6], **Merlin Airik**[8], **Rannar Airik**[8], **Radhika Muzumdar**[9], **Zhenwei Gong**[9], **Michel S. Torbenson**[10], **Edward V. Prochownik**[1,11,12,13,14,*]

[1]Division of Hematology/Oncology, UPMC Children's Hospital of Pittsburgh, Pittsburgh, PA 15224, USA

[2]The University of Pittsburgh School of Medicine, Pittsburgh, PA 15224, USA

[3]Tongji University School of Medicine, Shanghai, China

[4]Department of Developmental Biology, The University of Pittsburgh, Pittsburgh, PA, USA

[5]Central South University, Xiangya School of Medicine, Changsha, Hunan 410013, P.R. China

[6]Division of Medical Genetics, UPMC Children's Hospital of Pittsburgh, Pittsburgh, PA 15224, USA

[7]Division of Cardiology, The Department of Internal Medicine and the UPMC Aging Institute, Pittsburgh, PA 15224, USA

[8]Division of Nephrology, Children's Hospital of Pittsburgh, Pittsburgh, PA 15224, USA

[9]Division of Endocrinology, UPMC Children's Hospital of Pittsburgh, Pittsburgh, PA 15224, USA

[10]Division of Laboratory Medicine and Pathology, The Mayo Clinic, Rochester, MN 55905, USA

[11]Department of Microbiology and Molecular Genetics, UPMC, Pittsburgh, PA 15261, USA

[12]Hillman Cancer Center of UPMC, Pittsburgh, PA 15232, USA

[13]Pittsburgh Liver Research Center, UPMC, Pittsburgh, PA 15261, USA

[14]Lead contact



[*]Correspondence: procev@chp.edu.

AUTHOR CONTRIBUTIONS

E.V.P. conceived the study. H.W., Y.W., T.F., J.E.V., R. Airik, R.M., and E.V.P. designed experiments. H.W., J.L., T.S., A.R., J.M., B.M., R. Avula, Y.W., J.W., C.V.L., M.A., R. Airik, E.V.P., and Z.G. performed experiments and/or analyzed or interpreted data. H.W., J.M., and R. Airik analyzed transcriptomic data. H.W. and E.V.P. interpreted transcriptomic analyses. M.S.T. performed histopathologic analyses; H.W., J.L., and T.S. generated figures; E.V.P. and H.W. wrote the paper. All authors read and approved the final version of the manuscript prior to submission for publication.

DECLARATION OF INTERESTS

The authors declare no competing interests.

INCLUSION AND DIVERSITY

We support inclusive, diverse, and equitable conduct of research.

SUPPLEMENTAL INFORMATION

Supplemental information can be found online at https://doi.org/10.1016/j.celrep.2023.112830.

## SUMMARY

*MYC* proto-oncogene dysregulation alters metabolism, translation, and other functions in ways that support tumor induction and maintenance. Although $Myc^{+/-}$ mice are healthier and longer-lived than control mice, the long-term ramifications of more complete *Myc* loss remain unknown. We now describe the chronic consequences of body-wide *Myc* inactivation initiated postnatally. "*Myc*KO" mice acquire numerous features of premature aging, including altered body composition and habitus, metabolic dysfunction, hepatic steatosis, and dysregulation of gene sets involved in functions that normally deteriorate with aging. Yet, *Myc*KO mice have extended lifespans that correlate with a 3- to 4-fold lower lifetime cancer incidence. Aging tissues from normal mice and humans also downregulate Myc and gradually alter many of the same Myc target gene sets seen in *Myc*KO mice. Normal aging and its associated cancer predisposition are thus highly linked via Myc.


## In brief

Wang et al. show that the postnatal elimination of *Myc* causes premature aging and the deterioration of age-sensitive functions. Yet, these mice have extended lifespans and a reduced cancer incidence. Gradual Myc downregulation accompanies normal aging in many tissues. Thus, the strong relationship between aging and cancer can be severed by eliminating a single gene.

## Graphical Abstract

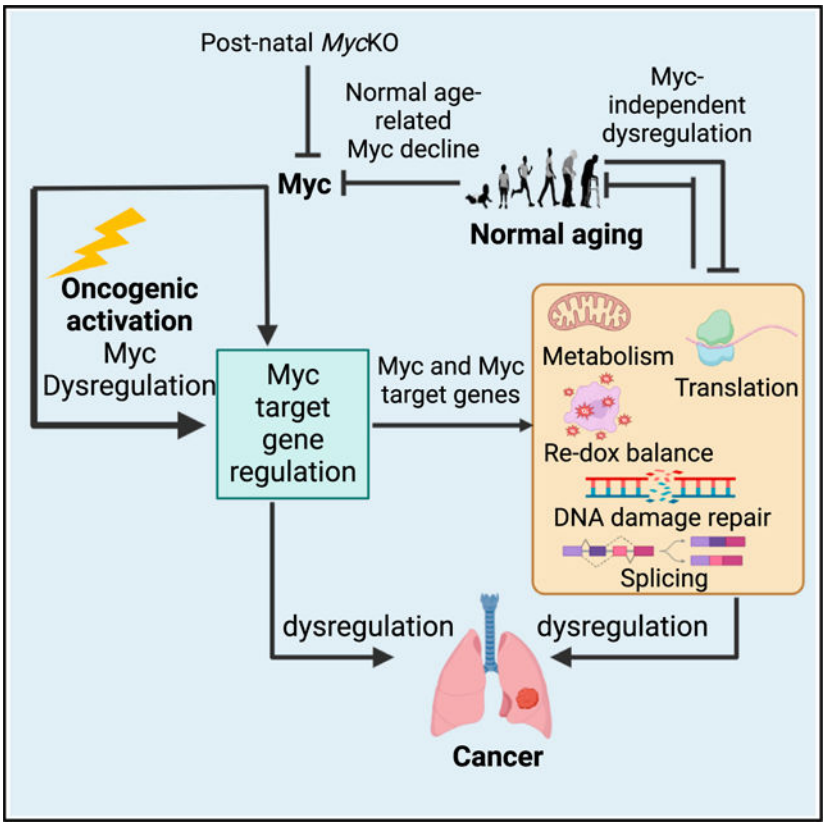

## INTRODUCTION

Precisely how the c-Myc oncoprotein (hereafter Myc) contributes to the pathogenesis of cancer has been well chronicled.[1,2] Tumors often deregulate *MYC*, which encodes a basic helixloop-helix-leucine zipper (bHLH-ZIP) transcription factor that, upon dimerizing with its partner protein Max, binds to "E boxes" in its target genes' promoters and enhances transcription.[3–7] Negative regulation by Myc-Max is mediated by interaction with and suppression of positively acting transcription factors such as Miz1.[6,8,9] Much Myc-mediated regulation involves context-dependent control over cell-cycle progression, metabolism, and translation.[4,6,10–14] The magnitude of each of these reflects Myc protein levels, its accessibility to and affinity for E boxes, and their occupancy by competing factors.[6,11] Secondary roles for Myc-mediated tumorigenesis include the promotion of angiogenesis and immune system evasion.[15–18] Continuous Myc expression is usually needed to maintain high rates of proliferation.[6,13,14,19–23]

Less is known about Myc's roles in normal development, since germline *Myc* inactivation in mice is embryonic lethal due to placental, hematopoietic, and vascular defects.[24–27] In adult mice, body-wide Myc inhibition by the dominant interfering "Omomyc" causes reversible aplastic anemia, colonic epithelial hypoplasia, and the regression of lung neoplasms.[21] However, neither the degree of Myc's incapacitation nor its long-term consequences were described. Tissue-specific *Myc* inactivation has demonstrated differential dependencies, although the observation times were again limited.[12,27–30] Thus, the long-term consequences of Myc inactivation remain unknown.

Relative to $Myc^{+/+}$ mice, $Myc^{+/-}$ mice viable, are smaller, age more slowly, have longer lifespans, and develop fewer age-related pathologies.[31] Their longevity may reflect a lower cancer incidence.[32,33] Whether survival was influenced by slower aging rather than altered Myc levels is unclear, since aging is the strongest independent predictor of cancer development.[31,32,34,35] These findings raise questions concerning Myc's role in maintaining normal body homeostasis and imply that the consequences of Myc loss are incremental.[27,31] The small number of transcript differences between $Myc^{+/-}$ and $Myc^{+/+}$ mouse tissues also suggested that half-normal levels of Myc can exert normal or near-normal control over its target genes.[11,31] Partial Myc expression might therefore forestall deleterious phenotypes in a dose-dependent manner.[27]

We describe here the body-wide, near-complete elimination of *Myc* initiated at weaning.[25,27] Unlike $Myc^{+/-}$ mice, "*Myc*KO" mice age prematurely yet live longer than wild-type (WT) mice while displaying a 3- to 4-fold lower lifetime cancer incidence. Transcriptional profiling in 3 tissues sensitive to *Myc* loss and/or aging shows widespread and early-onset dysregulation of genes involved in mitochondrial and ribosomal structure/function, oxidative stress, aging/senescence, DNA damage recognition/repair, and mRNA splicing, which is consistent with that in $Myc^{-/-}$ hepatocytes and murine embryonic fibroblasts (MEFs).[12–14,23,31,36–38] The transcriptomic changes resemble and precede by several months those arising during normal aging, including changes in both Myc itself and its target genes. The link between aging and cancer is therefore genetically maintained by Myc.

## RESULTS

### Near total-body *Myc*KO mice

B6.129S6-*Myc*$^{tm2Fwa}$/Mmjax mice[13,29] (Figures S1A and S1B) were crossed with B6.129-*Gt*(*ROSA*)*26Sortm1*(*cre/ERT2*)*Tyj/J* mice, which express a ROSA26-driven Cre recombinase-estrogen receptor (CreER) transgene.[39] Progeny strains with one or two copies of *CreER* were examined to determine how copy number influenced *Myc* excision efficiency initiated at weaning (*ca*. 4weeks). Because TaqMan-based assays (Figures S1A–S1D) performed 2 weeks after tamoxifen administration showed *Myc* locus excision efficiency in some cases to be dependent on *CreER* copy number (Figure S1E), subsequent studies were performed with mice carrying two copies of CreER (Figures S1E and S1F and Table S1). Tamoxifen-treated offspring of B6.129S6-*Myc*$^{tm2Fwa/}$/Mmjax 3 C57BL/6 mice with intact *Myc* genes served as wild-type (WT} controls. Myc transcript levels correlated well with the degree of *Myc* deletion (Figure S1E and Table S1). Follow-up qPCR/qRT-PCR studies indicated *Myc* loss persistence beyond 30 months, although in some tissues it was incomplete and less prominent (Figure S1F and Table S1). Myc protein was reduced in certain tissues with a proliferative compartment (Figures S1G and S1H).

### *Myc*KO mice age prematurely, survive longer, and have a lower cancer incidence

Growth rates and body masses of WT and *Myc*KO cohorts remained indistinguishable until ~10 months of age, when they diverged in both sexes. They then converged at 18–20 months, when body masses began their age-related decline (Figure 1A). *Myc*KO mice showed earlier decreases in lean mass and increases in adiposity and fat:lean mass ratios that explained the otherwise identical weights of younger mice. Thus, the overall body habitus of younger *Myc*KO mice prematurely assumed that of older WT mice.[40] In females, the differences became less pronounced as WT and *Myc*KO mice eventually acquired the same overall body composition. Although male *Myc*KO mice showed the same tendencies, the differences from WT mice persisted throughout life.

*Myc*KO mice developed alopecia and achromotrichia as early as 3–4 months of age, which first appeared peri-orbitally and/or peri-nasally (Figures 1B–1D and Video S1). In WT mice, achromotrichia comprised alternating dark and light gray hairs, whereas in *Myc*KO mice, all hairs were uniformly light gray, occurred in patches, and resembled those from melanocytespecific *Myc*KO mice (Figure 1E).[41,42] Some hair shafts also comprised alternating light-dark segments. Skin from alopecic areas showed epidermal thickening, hyperkeratinization, loss of surface invaginations, and reduced numbers of hair follicles and sebaceous glands (Figure S2A). Focal regions of perifollicular, senescence-associated b-galactosidase-positive cells were also noted (Figure S2B).

*Myc*KO mice, particularly younger males, were generally weaker, less coordinated, and less active (Figures 1F–1H). However, the magnitude of these differences, when they were first detected, and their duration were age-, sex-, and test-type dependent. For example, reduced grip strength, first noted in 3-month-old male *Myc*KO mice, did not persist beyond about 10 months (Figure 1F). This occurred in parallel with the premature muscle mass loss and its eventual equalization as WT mice aged (Figure 1A). Lessened ability to balance on a

Rotarod apparatus was noted in *Myc*KO mice of both sexes by 11 months and persisted in males (Figure 1G). Beginning at 13–16 months, male *MycKO* mice also showed less treadmill endurance (Figure 1H).[43] Finally, diurnal ambulatory activity of *Myc*KO mice was reduced in younger animals and decreased further by 20 months in *Myc*KO females (Figure 1I). *Myc*KO mice thus acquired age-related features and behaviors earlier than WT mice, although at different rates.[44–47] These differences either persisted or converged as WT mice aged.

Bone marrow failure accompanies *Myc* loss in both the embryo and the adult,[21,25,27] and *Myc*KO mice showed mild-moderate anemia and leukopenia within 10–15 days of initiating tamoxifen treatment (Figures S3A and S3B). The accompanying bone marrow hypoplasia reflected that this was well tolerated (Figure S3C). The peripheral findings resolved within several weeks despite the long-term persistence of *Myc* loss (Figures S3A and S3B).[21] However, the bone marrow of some *Myc*KO mice remained hypoplastic and resembled that of middle-aged normal animals (Figure S3C). Inactivating *Myc* prior to weaning and/or attaining weights of 15–16 g was associated with severe and usually fatal pancytopenia. Thus, the bone marrow's greatest Myc dependency declines during the first month of life.[27]

Myc loss is associated with transient flattening of the intestinal epithelium and abnormal crypts.[21,28,48] We observed similar changes in the colons in young *Myc*KO mice (*ca.* 2.5 months) that normalized by 5–6 months despite the persistence of *Myc* gene loss (Figure S3D).

Non-alcoholic fatty liver disease (NAFLD) increases in the context of age-related dyslipidemia, obesity, and insulin resistance.[36,49] Neutral lipid accumulation also follows Myc (and *Mycn*) loss/inhibition in a variety of cells and tissues and in livers lacking other members of the "Extended Myc Network" such as ChREBP and/or Mlx.[14,50–53] Yet, the contribution of aging to Myc-dependent NAFLD development is unknown.[13,14,29] Consistent with this, the neutral lipid and triglyceride content of 5-month-old *Myc*KO livers was higher than that of WT controls and rivaled that of even the oldest WT mice (Figure 2). These differences became less pronounced as the excess hepatic lipid in *Myc*KO livers was eventually matched by WT mice, indicating that *Myc*KO livers show acceleration of an otherwise normal age-related process.

Despite aging prematurely, *Myc*KO mice lived significantly longer than WT mice (Figure 3A). Postmortem necropsies showed that 58.1% of WT animals had tumors, with 64.3% of these resembling B cell lymphomas (Figure 3B).[33,34] These were frequently of high grade, were associated with hepatosplenomegaly, and often displayed leukemic dissemination. In contrast, only 17.3% of *Myc*KO mice had obvious tumors ($p < 0.0001$). The tumor spectra of the cohorts were similar, and in the few cases where mice had two or more tumors, they were histologically indistinguishable lymphomas (Figures 3C–3H). The 3.4-fold lower cancer incidence observed in *Myc*KO mice is consistent with the Myc dependency of most can-cers.[12–14,19,21,50,54] Thus, its most striking aspect was that it was dissociated from the premature aging phenotype.

Lymphomas involving 2 organs from 3 *Myc*KO mice were examined for Myc protein. Control tissues included a WT normal liver with low to undetectable endogenous Myc levels and a hepatoblastoma (HB) with high levels.[14,55] Myc levels in *Myc*KO lymphomas ranged from undetectable-low to severalfold higher than in HB (Figure 3I). Intact and amplified *Myc* gene loci were detected even when they expressed little protein (Figure 3J). Thus, some tumors arising in *Myc*KO mice originate in rare cells with intact *Myc* alleles that retain the ability to be amplified.

### *Myc*KO mice display metabolic and mitochondrial dysfunction

Age-related deterioration of mitochondrial structure and function affects organelle size, electron transport chain (ETC) activity, fatty acid β-oxidation (FAO), and redox balance, which are compounded by aging-related co-morbidities such as obesity, NAFLD, and insulin resistance.[37,56–63] Conversely, mitochondrial dysfunction and its excessive production of reactive oxygen species (ROS) can accelerate aging.[61,63,64] mtDNA and protein content and ETC function are reduced in individuals with type 2 diabetes, metabolic syndrome, and NAFLD.[62,65] Myc's roles in these processes include its maintenance of mitochondrial structure and function and the oxidation of glucose, glutamine, and fatty acids.[66–72] Linked to this is ROS overproduction in response to the ETC dysfunction associated with both over and underexpression of Myc.[69,71–74]

High nocturnal respiratory exchange ratios (RERs) of the youngest WT mice indicated near-complete reliance on glucose as the primary energy source (Figure 4A). Normally, RERs >1 are seen in juvenile mice and following post-starvation re-feeding, where they signify high levels of both *de novo* fatty acid synthesis (FAS) and glucose utilization.[75,76] The lower, adult-like nocturnal RERs of *Myc*KO mice during this time indicated their disproportionate reliance on FAO and/or reduced FAS efficiency. A glycolysis → FAO switch following hepatocyte-specific loss of Myc may increase fatty acid uptake in excess of that needed for FAO, with the difference being stored as neutral lipid that causes NAFLD (Figure 2).[13,14,23,29] The overreliance of *Myc*KO mice on FAO suggested the loss of Myc-dependent glycolysis, reduced provision of pyruvate for mitochondrial ATP production, or pyruvate's diversion into other pathways.[67,71,77–79] Regardless of the cause(s), the RERs of younger *Myc*KO mice resembled those of older animals. The differences persisted as mice aged but became more erratic, with the lower RERs of the latter now observed during the day.

WT and *Myc*KO RERs converged during fasting, indicating that both groups responded similarly when demands for FAO were high. Re-feeding was again associated with low *Myc*KO RERs, emphasizing the lifelong overreliance on FAO and/or suboptimal glucose utilization. *Myc*KO mice also showed higher levels of serum ketones in the face of normal glucose and lactate levels (Figure 4B). Finally, younger *Myc*KO mice episodically reduced water and food intake (Figure 4C and Data S1). While the latter might have forced a somewhat greater reliance on FAO in the youngest mice (Figure 4A), it seems unlikely that it fully explains the lower RERs, given that they persisted and were not associated with hypoglycemia (Figure 4B). Myc compromise thus promotes dysfunctional glycolysis and oxidative phosphorylation (Oxphos) and FAO dependency.[6,51–53,69,71,72]

Less efficient FAO accompanies aging and correlates with adiposity, NAFLD, ketosis, hyperglycemia, and insulin resistance.[60,80] In contrast, glycolytic and Oxphos dysfunction following Myc inhibition is accompanied by increased FAO that maintains ATP levels.[12,13,23,51,52,71,72,81] Lower RERs of young *Myc*KO mice might reflect an integration of these opposing factors that favors FAO. The convergence of aging WT and *Myc*KO RERs (Figure 4A) might also indicate a more rapid age-related decline in FAO in the latter group balanced by persistently high FAO needed to maintain dysfunctional mitochondria. Although baseline fasting glucose levels were similar in the two groups following a glucose challenge, younger *Myc*KO mice displayed the exaggerated hyperglycemia and hyperinsulinemia that characterizes type 2 diabetes (Figures 4B and 4D). *Myc*KO mice thus demonstrate defects in glucose metabolism consistent with their greater reliance on FAO. Eventual age-related metabolic compensation appears to be the result of other defects.

Liver, white adipose tissue, and skeletal muscle mitochondria from 5-month-old mice were assessed for complex I and II function.[12–14] Complex I responses of *Myc*KO liver and adipose tissue mitochondria were lower than those of WT mitochondria (Figure 4E). No differences were observed in succinate-driven complex II activities. In livers, where signals were sufficiently strong,[82] *Myc*KO palmitoyl CoA-driven oxygen consumption rates (OCRs) were again lower, thus suggesting a generalized complex I dysfunction.

Carnitine-long-chain fatty acid (LCFA) conjugation and the bidirectional transport of acyl carnitines across mitochondrial membranes are key steps in FAO.[83] Complex I disorders are associated with elevated serum levels of 3-hydroxy-C14-carnitine (C14-OH), which reflects inefficient LCFA oxidation.[83] Indeed, a mass spectrometry-based evaluation of 51 serum acylcarnitines in 5-month-old mice documented higher C14OH levels in the *Myc*KO group (Figures 4F and S4A). This difference disappeared by 20 months of age and was replaced by 12 new changes, mostly involving the accumulation of even longer chain (C16 and C18) serum acylcarnitines, suggesting a progressive deterioration of the FAO pathway in aging *Myc*KO mice akin to that of aging humans with type 2 diabetes (Figures 4G and S4B).[84] The normalization of C14-OH in this older cohort likely reflected reduced C14 pools resulting from accumulated longer-chain precursors and their defective oxidation to shorter-chain acylcarnitines. Aging cohorts continued to show aberrant serum acylcarnitine profiles that were consistent with the observed NAFLD, low RERs, and insulin resistance of young *Myc*KO mice (Figures 2, 4A, 4D, and S5). Twenty-month-old *Myc*KO mice also accumulated C5-carnitine (Figure S4B), suggesting errors in mitochondrial branched-chain amino acid (BCAA) catabolism and implying a broadening of energy-generating defects in aging *MycKO* mice.[85] Supporting this was a significant negative enrichment of FAO-related gene sets in 20-month-old *Myc*KO livers and negative enrichment in 5- and 20-month-old *Myc*KO mice for BCAA catabolic pathway-related gene sets (Figure 4H).

Blue native gel electrophoresis (BNGE) of ETC complexes and *in situ* enzymatic measurements showed no significant cohort- or age-related structural or functional differences (Figures 5A and 5B).[55,72,86] However, tissue- and age-dependent differences between WT and *Myc*KO mice were found among a subset of important and, in some cases, rate-limiting Myc-regulated glucose transporters and glycolytic enzymes (Figure 5C).[14,71,78,87] The Glut1 glucose transporter, whose gene is a Myc target,[78] and Glut4[87]

were regulated oppositely in 5-month-old *Myc*KO livers, whereas Glut2 did not change. Glut4 is expressed at low to undetectable levels in the liver, suggesting that it might be a negative Myc target.[87] This also appeared true in *Myc*KO skeletal muscle, where Glut4 is the major transporter.[87] Also demonstrating differences in expression between WT and *Myc*KO 5-month-old mice was the muscle-specific phosphofructokinase isoform PFK-M, which contrasted with no change in liver-specific PFK-L. Finally, pyruvate dehydrogenase (PDH) activity appeared to be increased in 5-month-old *Myc*KO livers by virtue of its reduced level of phosphorylation (pPDH), whereas in skeletal muscle, this activity was decreased.[79] Tissue-specific increases in PDH activity might represent responses to the impaired hepatic function of complex I that increases acetyl-coenzyme A availability and ETC activity (Figures 4E–4H).

Twenty-month-old mice also showed tissue-, cohort-, and age-specific differences (Figure 5C). Lower Glut1 levels originally observed in *Myc*KO livers and skeletal muscle persisted only in the latter tissue of older mice, whereas the initially higher levels of Glut4 expression in *Myc*KO mice remained elevated in both sets of older tissues. Elevated PFK-M levels also persisted. Neither PDH nor pPDH levels changed in livers, whereas pPDH levels in *Myc*KO skeletal muscle were reduced, as observed in 5-month-old livers.

Myc overexpression and underexpression both promote ROS.[23,72,74] In the former case, hyperactive mitochondria with a normal ETC simply generate more ROS, whereas in the latter case, ETC dysfunction increases electron "leakage."[69,70,88] *Myc*KO primary MEFs[23] generated more ROS and superoxide, indicating that disproportionate amounts originated in mitochondria (Figures 5D and 5E). These findings and others (Figures 4A, 4E, 4F, 4G, S4, and S5) argue that younger *Myc*KO mice acquire mitochondrial and ETC functional defects normally observed in aged WT mice.

## RNA-seq differences between WT and *Myc*KO tissues correlate with phenotypes

RNA sequencing (RNA-seq) was performed on liver, mesenteric white adipose tissue, and skeletal muscle from 5-month-old mice because they are Myc dependent for tissue homeostasis and/or because they undergo age-related changes (Figures 1A and 1B).[31,32,36–38,89] We first verified the dysregulation of multiple Myc target genes in these *Myc*KO tissues using gene set enrichment analysis (GSEA). The results were consistent with the previously documented inactivation of *Myc* (Figure S1E and Table S1), although enrichment patterns were tissue specific (Figures S6A–S6F).[14]

The paucity of gene expression differences between WT and $Myc^{+/-}$ tissues likely reflects low basal Myc levels in WT tissues and/or modest effects of Myc haploinsufficiency on high-affinity targets.[11,19,31] To capture the greatest possible variation among WT and *Myc*KO tissues, to avoid bias, and to identify functional categories, we performed GSEA. Seven particularly noteworthy categories were identified, with all having been previously identified in association with aging, senescence, or conditional Myc inactivation (Figures 6A and S7 and Data S1).[23,56–58,90–97]

The first category, "translation/ribosomal structure and function," contained gene sets encoding ribosomal subunits and factors involved in translation and the synthesis/processing

of rRNAs and tRNAs (Figures 6A and S7A). A second category, “mitochondrial structure and function,” encoded components of the mitochondrial membrane, the matrix, the ETC, and mitochondrial ribosomes (Figures 6A and S7B). We previously identified these categories in MEFs and hepatocytes lacking *Myc* and/or extended Myc network members.[6,12–14,23]

An “oxidative stress response” category (Figures 6A and S7C) encoded transcripts pertaining to the redox-responsive transcription factor NFE2L2/NRF2, the generation of superoxide, and the response to hydrogen peroxide previously documented in other *Myc*KO cells and tissues.[23,29,70,86]

Also, strongly dysregulated in 5-month-old *Myc*KO tissues were transcript categories associated with aging and senescence (Figures 6A, S7D, and S7E). A 79-member subset selected for its near-universal association with aging was also dysregulated in *Myc*KO liver and adipose tissue in ways that, again, marked them as possessing an “older” transcriptional profile (Figures 6B and 6C and Data S1). Also identified were gene sets known to be enriched in tissues from individuals with types 1 and 2 diabetes and cancer (Figures 6D and 6E and Data S1). In *Myc*KO tissues, the former sets were generally dysregulated in the directions seen in diabetic tissues, whereas in the latter, the directions of enrichment were opposite those seen in cancers and thus consistent with a low cancer risk (Figure 3B).

“DNA damage recognition and repair” comprised the sixth GSEA category in *Myc*KO tissues (Figures 6A and S7F). This category pertains to recognition/repair of radiation-induced lesions, DNA breaks and other damage, and telomere/shelterin complexes and was dysregulated in *Myc*KO MEFs, which show abnormal responses to DNA damage.[23] Monogenic disorders involving these genes include Werner syndrome, Nijmegen break syndrome, and “telomeropathies,” such as dyskeratosis congenita and aplastic anemia, which are associated with premature aging and cancer.[95,98–100] In most cases, genes in *Myc*KO tissues were enriched in the same direction as occurs in these human conditions and in *Myc*KO MEFs.[23] *Myc*KO livers also showed more double-stranded DNA breaks (Figure 6F). These findings indicate that Myc oversees interconnected pathways that participate in the recognition/repair of DNA damage and that are dysregulated in premature aging syndromes with high cancer susceptibility.

Enriched in *Myc*KO livers were gene sets encoding spliceosome components, which orchestrate intron-exon junction recognition, lariat formation/removal, and exon-exon ligation (Figures 6A and S7G).[101] However, we initially found no evidence increases in the frameshifts or indels that accumulate during aging and senescence as a result of aberrant splicing.[90,91,102]

## Myc target gene dysregulation in *Myc*KO mice occurs with normal aging

Knowing that ~10% of the transcript differences of $Myc^{+/-}$ mice originate from direct Myc targets,[31] we compared RNA-seq profiles of similarly aged WT and *Myc*KO cohorts. Focusing on previously enriched gene sets permitted two major observations. First, more differences existed between WT and *Myc*KO liver and adipose tissues at 5 months than at ~20 months (Figure 7A and Data S1). This indicated that much of the dysregulation of

young *Myc*KO tissues eventually occurred in older WT tissues, thus equalizing the previous differences. Indeed, many gene sets that distinguished the livers and adipose tissues of younger and older WT mice were dysregulated following Myc loss. This Myc-dependent transcript fingerprint of young mice was consistent with their age-related features (Figures 1A, 2, and 4).[32,36,76,94]

Muscle of young WT and *Myc*KO mice again showed much of the same Myc-dependent gene set enrichment previously seen in livers and adipose tissue (Figure 7A). However, many of these, notably in the "aging" category, were enriched in directions opposite those seen in livers and adipose tissue. Also seen was a more pronounced gene set enrichment in WT and *Myc*KO muscle at 20 months of age than in liver and adipose tissue and particularly for gene sets from the "translation/ribosomal structure and function" and "mitochondrial structure and function" categories. This suggested that GSEA differences in muscle were less equalized during aging. Indeed, the greater directional change in the enrichment of some gene sets in muscle, from down in young *Myc*KO mice to up in old mice, appeared to result from aging-related declines in WT mice (Figure 7A).

The 79-member aging-associated transcript set (Figures 6B and 6C and Data S1) was re-examined in older livers and adipose tissues, where differences between WT and *Myc*KO were again noted, although they were less pronounced than those of 5-month-old tissues (Figure 7B and Data S1). This again suggested that aging-related gene signatures associated with younger *Myc*KO tissues appear in WT tissues by 20 months of age.

More comprehensive assessments of types 1 and 2 diabetes-associated gene sets than used previously (Figure 6D) were performed on young and old tissues. Tissue-specific dysregulation of these was again observed among tissues from young mice (Figure 7C and Data S1). This persisted in older mice, although the numbers and identities of the gene sets and the enrichment levels changed in tissue-specific ways (Figure 7C). Thus, the dysregulation of these gene sets was already quite extensive in young *Myc*KO mice and remained so throughout life. Similar analyses of a larger number of gene sets associated with and/or deregulated in cancer also showed enrichment in MycKO tissues (Figures 6E and 7D and Data S1).

As already noted, the "RNA splicing" gene set category was enriched in young *Myc*KO livers but was unassociated with any changes in non-canonical mRNA splicing. Although only 8 such gene sets remained enriched at 20 months of age (Table S2), significant increases in non-canonically spliced transcripts were now observed (Figure 7E). Thus, aberrantly spliced transcripts accumulated only in older livers and thus likely required additional age-dependent and Myc-independent functions as well as tissue context.

A previous comparative study of young and old mice[103] showed significant age-related declines in Myc transcripts in 12 of 90 (13.3%) single-cell populations from 23 tissues (Figure 7F and Data S1). Thirty-five of 58 Myc target gene sets (60.3%) from the MSigDB database were also dysregulated in one or more single-cell populations of most of these tissues (Figure 7G and Data S1). Where the directionality of dysregulation could be determined, it usually correlated with the age-related declines in Myc levels. These

results thus documented extensive age-related alterations of direct Myc target gene transcript collections that would not have been anticipated based solely on Myc expression changes.

The above single-cell RNA-seq data were used to search the ENCODE and ChEA databases.[104,105] We found that 89.5% of genes whose expression changed significantly during normal aging were direct Myc targets, and 67.2% of chromatin immunoprecipitation sequencing (ChIP-seq)-confirmed direct Myc target genes from ENCODE and ChEA significantly altered their expression during aging (Figure 7H).

Myc expression also declines during the propagation of primary human fibroblasts, and the accompanying senescence can be prolonged or hastened by enforcing or inhibiting Myc, respectively.[23,106] Upon querying the GTEx database, which contains RNA-seq results from numerous normal human tissues, we found age-related declines in *Myc* expression to be common, particularly in adipose tissue, sigmoid colon, and leukocytes (Figure 7I). *Myc* transcripts were also lower in older individuals' fibroblasts, as noted previously in murine fibroblasts.[106,107] Consistent with Myc's role in maintaining the replication of most cell types, a previous study of >650 primary human fibroblast lines showed that those from older individuals become senescent sooner than those from younger individuals.[22,23,27,51,108] Interrogating the above samples with the collection of direct Myc target gene sets from the MSigDB database (Figures S6A–S6C) confirmed that positively regulated Myc target gene sets were negatively enriched in older tissues, and negatively regulated gene sets were positively enriched (Figure 7J). Thus, in both mice and humans, normal aging and senescence are commonly associated with Myc downregulation and appropriate changes in its target genes. The deliberate Myc inactivation and the ensuing dysregulation of its target genes in young *Myc*KO mice thus accelerated the changes that otherwise occur with normal aging.

## DISCUSSION

By postponing Myc inactivation until weaning, we have avoided the factors that contribute most strongly to prenatal demise while allowing ourselves to assess the consequences of its loss on multiple, interdependent whole-body phenotypes.[24,26,27] While differing from the method previously used to generate $Myc^{+/-}$ mice,[31] our approach permitted a comparison of the 2 mouse strains over their lifetimes.

*Myc*KO mice presented 2 disadvantages. First, *Myc*'s contributions to the substantial growth and development of the immediate postnatal period could not be determined (Figures S3A–S3C) (data not shown).[21] Second, the prominence of *Myc*KO phenotypes may be skewed in favor of tissues with the highest and most persistent *Myc* loss. The partial re-appearance of intact *Myc* alleles suggested that stem cell populations with incomplete *Myc* excision and proliferative advantages are responsible (Figure S1F and Table S1). Similarly, infrequent *Myc*KO mouse tumors appeared to originate from a minority population of cells that retained *Myc* (Figures 3I and 3J). *Myc*'s excisional variability might reflect the degree to which tamoxifen penetrates different tissues, the efficiency of its activation, and differential accessibility of the *Myc* locus to CreER.[109] Nonetheless, our approach provided a means to assess the life-long consequences of global *Myc* loss on health and fitness. Our studies

also demonstrate that some pathologies and phenotypes observed with tissue-specific and/or prenatal *Myc* inactivation are replicated when inactivation is delayed.[14,27,29,42] Certain phenotypes of $Myc^{+/-}$ mice that we did not observe, such as an overall reduced body size, are likely determined during embryogenesis.[27,31]

*Myc* inactivation in adults and juveniles causes bone marrow hypoplasia, peripheral cytopenias, colonic epithelial flattening, and villous atrophy (Figure S3).[21,24–28,110] While the other findings resolved, bone marrow continued to resemble that of aged mice (Figure S3C). The normal weights of young *Myc*KO mice and the absence of steatorrhea provided evidence that any malabsorption did not impair growth (Figure 1A and not shown). These observations point to Myc's variable importance at different developmental stages and that deleterious consequences of its loss are often mitigated when inactivation is delayed and/or incomplete.[6]

Relatively young *Myc*KO mice often displayed progressive age-related phenotypes. Appearing at different times and sometimes influenced by gender, they included increased fat:lean mass ratios, alopecia and achromotrichia, and reduced strength, endurance, and balance (Figure 1). Notable additional findings include NAFLD, glucose intolerance, and mitochondrial dysfunction, with a preferential reliance on FAO (Figures 1, 2, and 5D).[46,56,61,62,64] Mitochondrial abnormalities and steatosis occur in mice with hepatocyte-specific *Myc* loss of relatively short duration, with the current findings confirming and extending these earlier ones by showing that the maximal hepatic lipid content accumulates earlier in *Myc*KO mice (Figure 2).[13,14,29] Age-related changes in skin (Figure S2) also recapitulate some of the milder consequences of melanocyte-specific *Myc* KO.[42] Many of the abnormal phenotypes of *Myc*KO mice are thus attributable to interactions between Myc inactivation and normal aging phenotypes (Figure S8).

While the extended lifespan of $Myc^{+/-}$ mice was originally ascribed to a lower cancer incidence, their relative youthfulness may also have contributed.[31] Aging and cancer therefore remained temporally linked. Neoplasms are common in normal aging mice, and age is the strongest independent predictor of cancer development.[32,34,35] This association is exaggerated in human and murine disorders of premature aging despite the chronological youthfulness of affected individuals.[93,96,99,111,112] Highlighting this relationship is the critical contribution of Myc to cancer pathogenesis.[2,6,13–15] The lower lifetime cancer incidence of *Myc*KO mice (Figure 3B) indicates that its strict association with aging is maintained by a single gene, namely *Myc*. The reduced cancer incidence and increased longevity of *Myc*KO mice are even more remarkable given that several of their associated co-morbidities are independent risk factors for cancer development and shortened lifespan.[93,99,113–116]

Given Myc's link to cancer, the dissociation of aging and neoplasia in *Myc*KO mice raised the question of how occasional tumors do arise (Figure 3B).[11,13,14,54] The variable levels of their Myc expression suggested that at least some originated from a minority population of cells with intact Myc alleles (Figures 3I and 3J). Whether tumorigenesis in *Myc*KO mice is reduced due to a lower initiation rate or a slower growth rate (Figure 3B) requires further investigation, since roles for *Myc* in both steps have been

demonstrated.[13,14,19,23,54] Aside from *Myc*'s loss, indirect mechanisms may contribute to the low cancer incidence in *Myc*KO mice. These potentially include the suppression of Myc target genes by Max-Mxd family heterodimers or by cross-binding members of the Mlx Network.[6,14,117] *Myc*KO cells could have higher baseline rates of neoantigen generation resulting from DNA damage response/repair and mRNA splicing defects that could enhance immune surveillance (Figures 6A, 7A, 7E, S7F, and S7G).[23,118–120] Slower *Myc*KO tumor growth might allow for longer periods of neoantigen presentation and immune response maturation.[12–14] However, the degree to which anti-tumor immunity is actually enhanced might be limited given the Myc dependence of T cell expansion.[121]

The relationships among *Myc*, aging, and cancer likely cannot be explained by any single mechanism, since many of the gene sets under Myc's control functionally converge upon the "hallmarks" of both aging and cancer (Figures 6A, 7, and S8).[37,61,92,94,97,122–125] Both normal aging and Myc loss generate ROS production due to progressive ETC decline and/or increased reliance on FAO (Figures 4A and S8).[63,88,126] Excessive ROS and impaired ribosomal biogenesis/translation both accelerate aging.[97] Nuclear and mtDNA damage, aberrant splicing, and senescence also increase in the face of aging and *Myc* loss.[90,91,102,127–130] Genotoxic ROS also inhibit translation, thus highlighting how individual Myc- and/or age-linked functions crosstalk and influence one another (Figure S8).[131]

Do *Myc*KO mice better mimic normal aging than other models, which are largely based upon rare monogenic disorders of DNA damage recognition/repair?[132,133] Importantly, the aging of *Myc*KO mice directly reproduced the dysregulation of Myc target genes that normally accompanies aging in mice and humans and that correlates with declines in Myc itself (Figures 6 and 7). These findings indicate that *Myc* inactivation in juvenile mice prematurely re-creates the dysregulation of its downstream target genes and the aging-like deterioration of their collective functions with similar molecular and phenotypic outcomes (Figures 7F–7J and S8).

The aging-related enrichment of Myc target genes involved more tissues than did the declines in Myc. There are at least 3 explanations for this finding. First, in some tissues, *Myc* paralogs might play a larger role in regulating these gene sets. Although none of the above cells or tissues expressed significant levels of *Mycn*, some expressed Mycl, which sometimes declined during aging when *Myc* itself did not. Myc target gene sets may therefore be preferentially responsive to *Mycl* in certain tissues. Second, some Myc targets may be selectively sensitive to one or more Mxd proteins.[6,11] Finally, Mlx Network members might displace Myc-Max complexes in some tissues and modify Myc's transcriptional impact.[6,11]

"Heterozygous advantage" applies to genes such as those encoding α and β globins and the cystic fibrosis transmembrane conductance regulator, where single mutant alleles protect against malaria and diarrheal diseases, respectively, whereas mutational homozygosity can be lethal.[134–137] *Myc* hemizygosity's association with a spectrum of health benefits versus the pathologies of *MycKO* mice is consistent with *Myc* being a somewhat different example of heterozygous advantage, despite its association only in the experimental context

described here.[11,25,27,31] Nonetheless, single-nucleotide polymorphisms far upstream of the *Myc* coding region can significantly affect its expression and correlate with cancer susceptibilities.[138,139] Normal declines in *Myc* might thus have very different lifetime consequences depending upon its genetically predetermined initial levels. The heterozygous advantage of *Myc* might thus relate more to the genetic constraints upon its normal expression, which would become increasingly consequential as its levels decline with age and reach pathologic thresholds at different times.

Although inhibiting Myc to treat cancer has proved elusive, the finding that $Myc^{+/-}$ mice displayed increased longevity, a lower cancer incidence, and additional health dividends provides additional incentive to pursue this objective.[31,140–142] However, the current work suggests that caution is warranted in the use of Myc inhibitors, particularly to extend longevity.[143] Our work thus raises questions that will need to be confronted before such inhibitors can be employed clinically, particularly in children, where even short-term treatment with traditional chemotherapeutics can accelerate aging.[144] Among these is the degree to which Myc inhibition unintentionally accelerates aging, whether certain age-associated phenotypes will be differentially manifested, and whether some phenotypes can be "rejuvenated" when Myc expression is restored. Another question is whether *MycKO* phenotypes will appear when Myc inactivation is implemented later in life. Finally, might young age be a contraindication when cancer therapy demands that Myc inhibition be both efficient and prolonged? More refined evaluation in appropriate experimental and clinical settings will likely be necessary before answers to such questions are forthcoming.

### Limitations of the study

Among this study's unanswered questions are how the pathways that are affected by *Myc*'s loss cooperate to promote premature aging and the nature of their tissue dependencies (Figure S8). Myc-dependent alterations in mitochondrial and ribosomal structure and function, energy metabolism, and genome integrity drive both normal and premature aging. In our model, *Myc* inactivation is also not 100% efficient, and whether more complete *Myc* elimination remains compatible with extended longevity and allows better cataloging of all potential phenotypes remains unknown. Residual Myc expression may mask additional phenotypes, as seen with $Myc^{+/-}$ mice. In addition, those described here may be incomplete and/or milder than what is potentially achievable. Some tissues that were not carefully examined may also possess overlooked abnormalities. Finally, it remains unclear how delaying *Myc* inactivation until later in life affects the age-related findings we have reported.

## STAR★METHODS

### RESOURCE AVAILABILITY

**Lead contact—**All additional information and requests for resources, reagents, and methods should be directed to the lead contact, Edward V. Prochownik (procev@chp.edu).

**Materials availability—**All unique reagents generated in this study will be made available from the lead contact (E.V.P.) and may require a completed materials transfer agreement.

**Data and code availability—**All raw RNA-seq files have been deposited in the NCBI Gene Expression Omnibus[154] and are accessible through GEO Series accession number GSE223676 database (https://www.ncbi.nlm.nih.gov/geo/query/acc.cgi?acc=GSE223676 ). Data underlying the display items in the manuscript, related to Figures 1, 2, 3, 4, 5, 6, 7, and S1–S7 are available as Data S1 – Source data. The original full-length western blots for Figures 3I, 5C, and S1G have been deposited in Mendeley Data (https://doi.org/10.17632/4t9xbmxszn.1).

This paper does not report original code.

Any additional information required to reanalyze the data reported in this paper is available from the lead contact upon request.

## EXPERIMENTAL MODEL AND STUDY PARTICIPANT DETAILS

**Animal models—**Animal work was conducted in compliance with the Public Health Service Policy on Humane Care and Use of Laboratory Animal Research (ILAR) Guide for Care and Use of Laboratory Animals. All experimental procedures, diets and tests were approved by the Institutional Animal Care and Use Committee (IACUC) at the University of Pittsburgh. All mice were housed in a specific pathogenfree facility, maintained under standard conditions at UPMC Children's Hospital of Pittsburgh. The B6.129S6-*Myc*$^{tm2Fwa}$/Mmjax mouse strain, in which the second and third exons of the *Myc* gene are flanked by loxP sites, was originally obtained as a gift from I. Moreno de Alboran.[13,14,29] These were crossed with the B6.129-*Gt(ROSA)26Sortm1(cre/ERT2)Tyj*/J strain, which expresses a Cre recombinase-estrogen receptor (*CreER*) fusion transgene under the control of the ROSA26 promoter.[39]. 2 *Myc*$^{LoxP/LoxP}$ progeny strains were derived, containing one or 2 *CreER* transgene copies, which allowed for a determination of the efficiency of *Myc* excision in response to CreER dose. *CreER* activation and Myc excision were initiated at the time of weaning in mice that had attained a weight of 15 g or greater. Each mouse received 5 daily i.p. injections of freshly-prepared tamoxifen (75 mg/Kg) in corn oil. To ensure the complete metabolism and excretion of tamoxifen and to avoid any of its non-specific side effects, we allowed at least 8 wks before initiating any testing other than that specifically designed to confirm the extent of *Myc* exon 2 excision and full-length Myc transcript expression (Figure S1). As a further control for any long-term effects of tamoxifen treatment, control (WT) mice for all studies consisted of the offspring of matings between B6.129S6-*Myc*$^{tm2Fwa}$/Mmjax and wild-type C57BL/6 mice treated with tamoxifen in the manner described above. Equal numbers of males and female were used for all studies that were conducted during the entire lifetimes (Figure 3).

*Myc* excisional efficiency was determined using a quantitative TaqMan-based qPCR assay that compared the exon 2 : exon 1 ratio using tissues from the above mice and standard curves generated with known ratios of WT and *Myc*KO DNAs as described previously (Figures S1A–S1E).[13,14,29] Cre-ER transgene copy number was determined by a separate TaqMan-based assay using the primers listed in Figure S1D. 10 ng of total DNA was used in each TaqMan assay. 3 primer sets were designed to amplify regions to identify specifically unfloxed, floxed (WT) and *Myc*KO alleles. All primers and probes (Figure S1D) were synthesized by IDT, Inc. (Coralville, IA). PCR reactions were performed on CFX96

Touch™ Real-Time PCR Detection System (Bio-Rad, Inc.) using the following conditions: 95 °C for 5 min; 10 cycles at 95 °C for 20 s, and 65 °C~60 °C (decreasing by 0.5 °C per cycle) for 15 s, and 68°C for 10 s; 40 cycles at 95 °C for 15 s, and 60 °C for 1 min.

## METHOD DETAILS

**Derivation and propagation of primary murine embryo fibroblasts (MEFs)—** Briefly, 10–12 e14 embryos from pregnant WT mothers were decapitated, eviscerated, rinsed in PBS, placed into sterile 0.25% trypsin-EDTA and incubated 1 hr at 37C as described previously.[23,155] They were then finely minced and digested for an additional 1–2 h at 37C before transferring to fresh Dulbecco's modified minimum essential medium (DMEM) containing 10% FBS, 100 mM glutamine and penicillin/streptomycin as previously described.[69] After expanding for 3–4 days, these early passage cells were trypsinized and frozen at −80C to serve as subsequent stocks. These primary MEFs were designated as passage 1. To excise the floxed *Myc* alleles from the above cells, *in vitro* culturing was continued in fresh medium containing 500 nM 4-hydroxytamoxifen (4-OHT) (Sigma-Aldrich, St. Louis, MO), which was changed daily. On day 8 an aliquot of cells was harvested, DNA was isolated as described below and the ratio of WT and *Myc*KO Myc alleles was calculated using the same approach as described above for individual mouse tissues. Under these conditions, *Myc* allele excision routinely exceeded 95%.[23]

**Strength and endurance testing—**Strength testing was performed using a Grip Strength Meter (Harvard Apparatus, Holliston, MA) according to the direction of the supplier. Rotarod testing (SPW Industrial, Laguna Hills, CA) was based on a modification of the standard operating procedure from Jackson Laboratories: https://www.jax.org/-/media/jaxweb/files/research-and-faculty/tools-and-resources/peripheral-neuropathy-resource/rotarod.pdf?la=en&hash=78228ECB294E38BC773843500CDE2E8C99A96316. Briefly, animals were initially placed on the slowly rotating rod (5 rpm) and maintained at this speed for 20 sec. The speed was then increased by 5 rpm increments each lasting 20 sec. The recorded numbers indicate the total time that each mouse was able to maintain its balance.

**Treadmill performance—**Treadmill performance was monitored with a Columbus Instruments Exer 3/6 apparatus (Columbus, OH). Groups of 6 mice at a time (3 WT and 3 *Myc*KO) were evaluated according to a published protocol.[156] Briefly, mice were allowed to run along a treadmill (elevated 10° from the horizontal) at a gradually increasing pace until reaching exhaustion, which was defined as the time at which they preferred to rest for >5 sec. upon an immobile metal shock plate at the bottom of the treadmill. The total distance run until reaching the point of exhaustion was recorded for each animal.

**Metabolic cage profiling—**These were performed essentially as described previously.[29] Briefly, control and *Myc*KO mice of the indicated ages were housed individually in metabolic cages (Columbus Instruments) and allowed to acclimate for 24 hr while being provided ad *lib* access to water and a standard mouse chow containing 5% fat (Picolab 5053; LabDiet, St. Louis, MO, USA). $VO_2$ and $VCO_2$ were recorded every 20 min over the subsequent 48 hr along with food intake and overall activity. At the conclusion of

this observation period, mice were starved overnight (12 hr) and then provided with a standard diet for 24 hr followed by a high-fat diet (45%) for an additional 24 hr while again monitoring RERs. Data analyses were performed with a web-based analysis software package CalR (https://calrapp.org/cite.html).

**Glucose tolerance tests and serum glucose, lactate, and ketone measurements—**Mice were fasted for 5 hr. at which time whole blood glucose, lactate and ketone levels were obtained using meters and compatible strips according to the directions provided by the suppliers (Glucose AimStrip Plus, Germaine Laboratories, Inc. San Antonio, TX; Lactate Plus Analyzer, Sports Resource Group, Inc., Hawthorne NY; Keto-Mojo Ketone Meter, Keto-Check, Inc. Napa, CA). To perform glucose tolerance tests and to measure insulin levels, the above mice were injected with 2g of dextrose/kg body mass with blood glucose levels being subsequently measured at the indicated times. Serum insulin levels were measured using an Ultra Sensitive Mouse Insulin ELISA Kit according to the directions provided by the supplier (Crystal Chem, Elk Grove Village, IL).

**ImageJ quantification of ORO staining—**ORO- and hematoxylin-stained tissue sections were imaged on a Leica DFC7000T microscope with 5x and 40x magnification. Multiple overlapping images of each section were acquired for the full area. The images of each section were joined using the stitching plugin of the open source software FIJI.[157–159] After subtracting background from each image, color de-convolution[160] was performed in FIJI where the colors were specified in advance from ROIs respectively corresponding to unstained tissue, strongly stained tissue and the slide background. Quantification of Oil-Red-O positive staining was performed as described in ImageJ documentation (https://imagej.nih.gov/ij/docs/examples/stained-sections/index.html). Higher resolution images were acquired at 5x magnification(Figure 2C).

**Nucleic acid isolation—**DNAs and RNAs were isolated from mouse tissues using DNeasy and RNeasy kits, respectively according to the directions of the supplier (Qiagen, Inc. Germantown, MD). Exceptions to this were made in the case of adipose tissue and skeletal muscle for which we utilized a RNeasy Lipid Tissue extraction Kit and QIAzol Lysis Reagent (Qiagen, Inc., Germantown, MD), respectively. Total RNAs were reverse transcribed using a SuperScript IV First-Strand Synthesis System according to the directions of the supplier (Thermo Fisher Scientific, Pittsburgh, PA). To determine the degree of Myc transcript reduction in control and *Myc*KO tissues, 2 separate TaqMan-based qRT-PCR assays were performed that compared the exon 2: exon 1 ratio signals in each WT and *Myc*KO tissue (Figures S1D and S1E).

**Blue native gel electrophoresis (BNGE), *in situ* enzymatic assays for ETC enzymatic function—**Non-denaturing gel electrophoresis was performed largely as described previously.[55,72] Briefly, purified mitochondria (approx. 1 mg of total protein), were lysed by the addition of digitonin and then incubated on ice for 20 min. Coomassie blue solution (5% Coomassie blue G250 in 750 mM 6-aminocaproic acid) was added and the suspension was then centrifuged at 14,000 × *g* for 20 min at 4°C. The supernatant was diluted in the supplier's buffer, loaded onto a 3–12% Native PAGE Novex Bis-Tris

gel (Life Technologies, Carlsbad, CA) and electrophoresed for 4 hr at 4C at 80 V. Gels were then stained with Bio-Safe Coomassie G250 (Bio-Rad, Hercules, CA) for 30 min and de-stained exhaustively in deionized water. Stained gels were scanned and the imaged using an AlphaEaseFC 2200 scanner and AlphaEaseFC software. Enzymatic assays for mitochondrial complexes and super-complexes were performed as previously described for Complex I (NADH ubiquinone oxidoreductase), Complex III (CIII) (decylubiquinol cytochrome c oxidoreductase), Complex IV (CIV) (cytochrome c oxidase) and Complex V (ATPase).[72] Band intensities were measured and quantified using Image J software and normalized with their corresponding bands on the Coomassie stained blue native gel.

**ROS assessment—**CM-$H_2$DCFDA and MitoSOX™ Red dyes were utilized to measure reactive oxygen species (ROS) levels (Molecular Probes, Eugene, OR, USA) according to the manufacturer's protocol. This was achieved by exposing monolayer cultures of mouse embryonic fibroblasts (MEFs) maintained at a temperature of 37 °C. Quantifications were performed on 6 biological replicates comprising 20,000 cells/sample using a BD LSRII flow cytometer (Becton-Dickinson Biosciences, San Jose, CA, USA) and results were analyzed using FlowJo v10 software. This was done as described in Wang et al.[23]

**β-galactosidase staining—**Tissue sections were stained for β-galactosidase using a Senescence Detection Kit (ab65351) according to the directions of the supplier (Abcam, Inc., Waltham, MA).

**SDS-polyacrylamide gel electrophoresis (SDS-PAGE) and immunoblotting—**At the time of sacrifice, individual tissues were removed, and immediately placed on ice. They were then divided into small sections, snap-frozen in liquid nitrogen and maintained at −80C for long-term storage. To prepare samples for SDS page, tissue fragments were disrupted in PAGE buffer using a Bullet Blender as previously described.[55,161] Protein concentration was quantified using the Bradford reagent (Bio-Rad, Inc., Hercules, CA). Electrophoresis, semi-dry blotting and protein detection was performed as previously described.[55] Antibodies used for the detection of specific proteins were used largely according to the directions of the suppliers and are shown in Table S3.

**Immunohistochemistry and immunohistofluorescence staining—**All tissues were fixed in 10% formalin, paraffin embedded and cut into 4 μm thick sections for standard hematoxylin/eosin staining or immunostaining procedures as previously described (Wang 2022). Prior to staining for Myc, heat-induced antigen retrieval was performed using a citrate buffer (pH 6.0) for 30 minutes. Sections were incubated with a rabbit anti-Myc antibody (1:250; N262, SantaCruz) at 4C for 72 hours. A biotinylated secondary antibody was used to amplify the signal using an avidin–biotin substrate (Vector Laboratories, Inc., Newark, CA). Immunohistofluorescence staining for γH2AX was done as described in Wang et al[23].

**Transcriptional profiling—**RNAs were purified from omental adipose tissue, liver and skeletal muscle as described above followed by DNAase digestion.[13,14,23] RIN values were determined using an Agilent 2100 Bioanalyzer (Agilent Technologies, Foster City, CA) and only those with values of >8.5 were processed further. Sequencing libraries were generated

with a NEBNext Ultra Directional RNA Library Prep kit according to the supplier's directions (New England Biolabs, Beverly, MA). Sequencing was performed as previously described on a NovaSeq 600 instrument (Illumina, Inc., San Diego, CA) by Novagene, Inc. (Sacramento, CA).[13,14,23] Original data were deposited in the NCBI Gene Expression database and are available through the Gene Expression Omnibus (GEO)[154] under accession number GSE223676.

To identify differentially expressed transcripts, we utilized CLC Genomic Workbench version 21(Qiagen) and mapped raw reads to the GRCm38.p6 mouse reference genome. Functionally related and differentially expressed groups were identified using clusterProfiler (R package version 4.2)[149,150] by first screening the MSigDB data bases (http://www.gseamsigdb.org/gsea/msigdb/as described previously.[13,14] We also screened the Enrichr collection to identify additional groups of gene sets that were either absent from or underrepresented in MSigDB (http://amp.pharm.mssm.edu/Enrichr).[146–148] Representative gene sets along with their normalized enrichment score (NES) and q values were displayed graphically using the Ridgeline plot application from Clusterprofiler (https://rdrr.io/bioc/enrichplot/man/ridgeplot.html).

To identify non-canonically spliced transcripts, we utilized the nf-core/rnaseq-3.4 analysis pipeline with the percentage of non-canonical splices being calculated from multi-qc of STAR section pct_noncanonical_splices = num_noncanonical_splices/total_reads*100.[151,152] Tabula Muris Consortium mosue single cell RNAseq data to evaluate the expression of Myc and Myc targets expression were obtained from https://figshare.com/ndownloader/files/27856758 and analyzed as described.[103,162] Myc transcript levels in tissues obtained from young and old human tissues were downloaded from the GTEx Portal (GTEx Analysis V8 release: RNAseq gene TPMs by tissue) (https://gtexportal.org/home/datasets dbGaP: phs000424.v8.p2).[163]

### QUANTIFICATION AND STATISTICAL ANALYSIS

Quantification and statistical analysis were performed using R software v4.2.0[164] (R Foundation for Statistical Computing, Vienna, Austria) and GraphPad Prism v9.00 (GraphPad Software Inc., USA). The ComplexHeatmap and ggplot2 packages were utilized for boxplot and heatmap visualizations, while the survminer package was used for survival curve plotting. The number of samples per group (n) for each experiment is indicated either in the figure legend or within the figure itself. A two-tailed, unpaired t-test was employed to assess significant differences between normally distributed populations, while a two-tailed Mann-Whitney exact test was used for non-normally distributed populations. A p-value below 0.05 was considered statistically significant. Significance is denoted as follows: * = $p < 0.05$, ** = $p < 0.01$, *** = $p < 0.001$, **** = $p < 0.0001$, and "ns" indicates not significant. Detailed statistical analysis information can also be found in each figure legend.

## Supplementary Material

Refer to Web version on PubMed Central for supplementary material.

## ACKNOWLEDGMENTS

This work was supported by NIH grant RO1 CA174713, a Hyundai Hope on Wheels Scholar grant, Rally Foundation Independent Investigator grant 22IN42, and The UPMC Children's Hospital of Pittsburgh Foundation (all to E.V.P). J.E.V. was supported by NIH grant DK RO1 109907. M.S.T. was supported by NIH grant P50 CA 210964. Analysis of RNA-seq data was partly supported by The University of Pittsburgh Center for Research Computing. Acylcarnitine profiling was performed in collaboration with the Rangos Research Center Metabolic Core LC/MS/MS services at the Department of Pediatrics, University of Pittsburgh Medical Center.

## REFERENCES

1. Kalkat M, De Melo J, Hickman KA, Lourenco C, Redel C, Resetca D, Tamachi A, Tu WB, and Penn LZ (2017). MYC deregulation in primary human cancers. Genes 8, 151. 10.3390/genes8060151. [PubMed: 28587062]
2. Nesbit CE, Tersak JM, and Prochownik EV (1999). MYC oncogenes and human neoplastic disease. Oncogene 18, 3004–3016. 10.1038/sj.onc.1202746. [PubMed: 10378696]
3. Ge Z, Leighton JS, Wang Y, Peng X, Chen Z, Chen H, Sun Y, Yao F, Li J, Zhang H, et al. (2018). Integrated genomic analysis of the ubiquitin pathway across cancer types. Cell Rep. 23, 213–226.e3. 10.1016/j.celrep.2018.03.047. [PubMed: 29617661]
4. Dang CV, O'Donnell KA, Zeller KI, Nguyen T, Osthus RC, and Li F. (2006). The c-Myc target gene network. Semin. Cancer Biol 16, 253–264. 10.1016/j.semcancer.2006.07.014. [PubMed: 16904903]
5. Kalkat M, Resetca D, Lourenco C, Chan PK, Wei Y, Shiah YJ,Vitkin N, Tong Y, Sunnerhagen M, Done SJ, et al. (2018). MYC protein interactome profiling reveals functionally distinct regions that cooperate to drive tumorigenesis. Mol. Cell 72, 836–848.e7. 10.1016/j.molcel.2018.09.031. [PubMed: 30415952]
6. Prochownik EV (2022). Regulation of normal and neoplastic proliferation and metabolism by the extended myc network. Cells 11. 10.3390/cells11243974.
7. Rahl PB, Lin CY, Seila AC, Flynn RA, McCuine S, Burge CB, Sharp PA, and Young RA (2010). c-Myc regulates transcriptional pause release. Cell 141, 432–445. 10.1016/j.cell.2010.03.030. [PubMed: 20434984]
8. Gartel AL, and Shchors K. (2003). Mechanisms of c-myc-mediated transcriptional repression of growth arrest genes. Exp. Cell Res 283, 17–21. 10.1016/s0014-4827(02)00020-4. [PubMed: 12565816]
9. Herkert B, and Eilers M. (2010). Transcriptional repression: the darkside of myc. Genes Cancer 1, 580–586. 10.1177/1947601910379012. [PubMed: 21779459]
10. Gomez-Roman N, Felton-Edkins ZA, Kenneth NS, Goodfellow SJ,Athineos D, Zhang J, Ramsbottom BA, Innes F, Kantidakis T, Kerr ER, et al. (2006). Activation by c-Myc of transcription by RNA polymerases I, II and III. Biochem. Soc. Symp 73, 141–154. 10.1042/bss0730141.
11. Prochownik EV, and Wang H. (2022). Normal and neoplastic growth suppression by the extended myc network. Cells 11. 10.3390/cells11040747.
12. Wang H, Lu J, Edmunds LR, Kulkarni S, Dolezal J, Tao J, Ranganathan S, Jackson L, Fromherz M, Beer-Stolz D, et al. (2016). Coordinated activities of multiple myc-dependent and myc-independent biosynthetic pathways in hepatoblastoma. J. Biol. Chem 291, 26241–26251. 10.1074/jbc.M116.754218. [PubMed: 27738108]
13. Wang H, Dolezal JM, Kulkarni S, Lu J, Mandel J, Jackson LE, Alencastro F, Duncan AW, and Prochownik EV (2018). Myc and ChREBP transcription factors cooperatively regulate normal and neoplastic hepatocyte proliferation in mice. J. Biol. Chem 293, 14740–14757. 10.1074/jbc.RA118.004099. [PubMed: 30087120]
14. Wang H, Lu J, Alencastro F, Roberts A, Fiedor J, Carroll P, Eisenman RN, Ranganathan S, Torbenson M, Duncan AW, and Prochownik EV (2022). Coordinated cross-talk between the myc and mlx networks in liver regeneration and neoplasia. Cell. Mol. Gastroenterol. Hepatol 13, 1785–1804. 10.1016/j.jcmgh.2022.02.018. [PubMed: 35259493]
15. Gabay M, Li Y, and Felsher DW (2014). MYC activation is a hallmark of cancer initiation and maintenance. Cold Spring Harb. Perspect. Med 4, a014241. 10.1101/cshperspect.a014241.

16. Kress TR, Pellanda P, Pellegrinet L, Bianchi V, Nicoli P, Doni M,Recordati C, Bianchi S, Rotta L, Capra T, et al. (2016). Identification of MYC-dependent transcriptional programs in oncogene-addicted liver tumors. Cancer Res. 76, 3463–3472. 10.1158/00085472.CAN-16-0316. [PubMed: 27197165]

17. Soucek L, and Evan GI (2010). The ups and downs of Myc biology.Curr. Opin. Genet. Dev 20, 91–95. 10.1016/j.gde.2009.11.001. [PubMed: 19962879]

18. Swaminathan S, Hansen AS, Heftdal LD, Dhanasekaran R, Deutzmann A, Fernandez WDM, Liefwalker DF, Horton C, Mosley A, Liebersbach M, et al. (2020). MYC functions as a switch for natural killer cell-mediated immune surveillance of lymphoid malignancies. Nat. Commun 11, 2860. 10.1038/s41467-020-16447-7. [PubMed: 32503978]

19. Dolezal JM, Wang H, Kulkarni S, Jackson L, Lu J, Ranganathan S, Goetzman ES, Bharathi SS, Beezhold K, Byersdorfer CA, and Prochownik EV (2017). Sequential adaptive changes in a c-Myc-driven model of hepatocellular carcinoma. J. Biol. Chem 292, 10068–10086. 10.1074/jbc.M117.782052. [PubMed: 28432125]

20. Mateyak MK, Obaya AJ, Adachi S, and Sedivy JM (1997). Phenotypes of c-Myc-deficient rat fibroblasts isolated by targeted homologous recombination. Cell Growth Differ. 8, 1039–1048. [PubMed: 9342182]

21. Soucek L, Whitfield J, Martins CP, Finch AJ, Murphy DJ, Sodir NM, Karnezis AN, Swigart LB, Nasi S, and Evan GI (2008). Modelling Myc inhibition as a cancer therapy. Nature 455, 679–683. 10.1038/nature07260. [PubMed: 18716624]

22. Wang H, Mannava S, Grachtchouk V, Zhuang D, Soengas MS,Gudkov AV, Prochownik EV, and Nikiforov MA (2008). c-Myc depletion inhibits proliferation of human tumor cells at various stages of the cell cycle. Oncogene 27, 1905–1915. 10.1038/sj.onc.1210823. [PubMed: 17906696]

23. Wang H, Stevens T, Lu J, Airik M, Airik R, and Prochownik EV(2022). Disruption of multiple overlapping functions following stepwise inactivation of the extended myc network. Cells 11. 10.3390/cells11244087.

24. Baudino TA, McKay C, Pendeville-Samain H, Nilsson JA, Maclean KH, White EL, Davis AC, Ihle JN, and Cleveland JL (2002). c-Myc is essential for vasculogenesis and angiogenesis during development and tumor progression. Genes Dev. 16, 2530–2543. 10.1101/gad.1024602. [PubMed: 12368264]

25. Davis AC, Wims M, Spotts GD, Hann SR, and Bradley A. (1993). Anull c-myc mutation causes lethality before 10.5 days of gestation in homozygotes and reduced fertility in heterozygous female mice. Genes Dev. 7, 671–682. 10.1101/gad.7.4.671. [PubMed: 8458579]

26. Dubois NC, Adolphe C, Ehninger A, Wang RA, Robertson EJ,and Trumpp A. (2008). Placental rescue reveals a sole requirement for c-Myc in embryonic erythroblast survival and hematopoietic stem cell function. Development 135, 2455–2465. 10.1242/dev.022707. [PubMed: 18550708]

27. Trumpp A, Refaeli Y, Oskarsson T, Gasser S, Murphy M, Martin GR, and Bishop JM (2001). c-Myc regulates mammalian body size by controlling cell number but not cell size. Nature 414, 768–773. 10.1038/414768a. [PubMed: 11742404]

28. Bettess MD, Dubois N, Murphy MJ, Dubey C, Roger C, Robine S, and Trumpp A. (2005). c-Myc is required for the formation of intestinal crypts but dispensable for homeostasis of the adult intestinal epithelium. Mol. Cell Biol 25, 7868–7878. 10.1128/MCB.25.17.7868-7878.2005. [PubMed: 16107730]

29. Edmunds LR, Otero PA, Sharma L, D'Souza S, Dolezal JM, David S, Lu J, Lamm L, Basantani M, Zhang P, et al. (2016). Abnormal lipid processing but normal long-term repopulation potential of myc−/− hepatocytes. Oncotarget 7, 30379–30395. 10.18632/oncotarget.8856 . [PubMed: 27105497]

30. Rosselot C, Kumar A, Lakshmipathi J, Zhang P, Lu G, Katz LS,Prochownik EV, Stewart AF, Lambertini L, Scott DK, and Garcia-Ocaña A. (2019). Myc is required for adaptive beta-cell replication in young mice but is not sufficient in one-year-old mice fed with a high-fat diet. Diabetes 68, 1934–1949. 10.2337/db18-1368. [PubMed: 31292135]

31. Hofmann JW, Zhao X, De Cecco M, Peterson AL, Pagliaroli L,Manivannan J, Hubbard GB, Ikeno Y, Zhang Y, Feng B, et al. (2015). Reduced expression of MYC increases longevity and enhances healthspan. Cell 160, 477–488. 10.1016/j.cell.2014.12.016 . [PubMed: 25619689]

32. Pettan-Brewer C, and M Treuting P. (2011). Practical pathology of aging mice. Pathobiol. Aging Age Relat. Dis 1, 7202. 10.3402/pba.v1i0.7202.
33. Ward JM (2006). Lymphomas and leukemias in mice. Exp. Toxicol. Pathol 57, 377–381. 10.1016/j.etp.2006.01.007. [PubMed: 16713211]
34. Snyder JM, Ward JM, and Treuting PM (2016). Cause-of-Death analysis in rodent aging studies. Vet. Pathol 53, 233–243. 10.1177/0300985815610391. [PubMed: 26508696]
35. White MC, Holman DM, Boehm JE, Peipins LA, Grossman M,and Henley SJ (2014). Age and cancer risk: a potentially modifiable relationship. Am. J. Prev. Med 46, S7–S15. 10.1016/j.amepre.2013.10.029. [PubMed: 24512933]
36. Honma T, Yanaka M, Tsuduki T, and Ikeda I. (2011). Increased lipid accumulation in liver and white adipose tissue in aging in the SAMP10 mouse. J. Nutr. Sci. Vitaminol 57, 123–129. 10.3177/jnsv.57.123. [PubMed: 21697630]
37. Short KR, Bigelow ML, Kahl J, Singh R, Coenen-Schimke J,Raghavakaimal S, and Nair KS (2005). Decline in skeletal muscle mitochondrial function with aging in humans. Proc. Natl. Acad. Sci. USA 102, 5618–5623. 10.1073/pnas.0501559102. [PubMed: 15800038]
38. Uchitomi R, Hatazawa Y, Senoo N, Yoshioka K, Fujita M, Shimizu T, Miura S, Ono Y, and Kamei Y. (2019). Metabolomic analysis of skeletal muscle in aged mice. Sci. Rep 9, 10425. 10.1038/s41598-019-46929-8. [PubMed: 31320689]
39. Ventura A, Kirsch DG, McLaughlin ME, Tuveson DA, Grimm J,Lintault L, Newman J, Reczek EE, Weissleder R, and Jacks T. (2007). Restoration of p53 function leads to tumour regression in vivo. Nature 445, 661–665. 10.1038/nature05541. [PubMed: 17251932]
40. Pappas LE, and Nagy TR (2019). The translation of age-related bodycomposition findings from rodents to humans. Eur. J. Clin. Nutr 73, 172–178. 10.1038/s41430-018-0324-6. [PubMed: 30283153]
41. Fernandez-Flores A, Saeb-Lima M, and Cassarino DS (2019). Histopathology of aging of the hair follicle. J. Cutan. Pathol 46, 508–519. 10.1111/cup.13467. [PubMed: 30932205]
42. Pshenichnaya I, Schouwey K, Armaro M, Larue L, Knoepfler PS, Eisenman RN, Trumpp A, Delmas V, and Beermann F. (2012). Constitutive gray hair in mice induced by melanocyte-specific deletion of c-Myc. Pigment Cell Melanoma Res. 25, 312–325. 10.1111/j.1755-148X.2012.00998.x. [PubMed: 22420299]
43. Goh J, and Ladiges W. (2015). Voluntary wheel running in mice.Curr. Protoc. Mol. Biol 5, 283–290. 10.1002/9780470942390.mo140295.
44. Dall'Ara E, Boudiffa M, Taylor C, Schug D, Fiegle E, Kennerley AJ, Damianou C, Tozer GM, Kiessling F, and Müller R. (2016). Longitudinal imaging of the ageing mouse. Mech. Ageing Dev 160, 93–116. 10.1016/j.mad.2016.08.001. [PubMed: 27530773]
45. Howlett SE (2015). Assessment of frailty in animal models. Interdiscip. Top. Gerontol. Geriatr 41, 15–25. 10.1159/000381131. [PubMed: 26301976]
46. Ponti F, Santoro A, Mercatelli D, Gasperini C, Conte M, Martucci M, Sangiorgi L, Franceschi C, and Bazzocchi A. (2019). Aging and imaging assessment of body composition: from fat to facts. Front. Endocrinol 10, 861. 10.3389/fendo.2019.00861.
47. Whitehead JC, Hildebrand BA, Sun M, Rockwood MR, Rose RA, Rockwood K, and Howlett SE (2014). A clinical frailty index in aging mice: comparisons with frailty index data in humans. J. Gerontol. A Biol. Sci. Med. Sci 69, 621–632. 10.1093/gerona/glt136. [PubMed: 24051346]
48. Muncan V, Sansom OJ, Tertoolen L, Phesse TJ, Begthel H, Sancho E, Cole AM, Gregorieff A, de Alboran IM, Clevers H, and Clarke AR (2006). Rapid loss of intestinal crypts upon conditional deletion of the Wnt/Tcf-4 target gene c-Myc. Mol. Cell Biol 26, 8418–8426. 10.1128/MCB.00821-06. [PubMed: 16954380]
49. Bertolotti M, Lonardo A, Mussi C, Baldelli E, Pellegrini E, Ballestri S, Romagnoli D, and Loria P. (2014). Nonalcoholic fatty liver disease and aging: epidemiology to management. World J. Gastroenterol 20, 14185–14204. 10.3748/wjg.v20.i39.14185. [PubMed: 25339806]
50. Müller I, Larsson K, Frenzel A, Oliynyk G, Zirath H, Prochownik EV, Westwood NJ, and Henriksson MA (2014). Targeting of the MYCN protein with small molecule c-MYC inhibitors. PLoS One 9, e97285. 10.1371/journal.pone.0097285.

51. Wang H, Sharma L, Lu J, Finch P, Fletcher S, and Prochownik EV(2015). Structurally diverse c-Myc inhibitors share a common mechanism of action involving ATP depletion. Oncotarget 6, 15857–15870. 10.18632/oncotarget.4327. [PubMed: 26036281]
52. Wang H, Teriete P, Hu A, Raveendra-Panickar D, Pendelton K, Lazo JS, Eiseman J, Holien T, Misund K, Oliynyk G, et al. (2015). Direct inhibition of c-Myc-Max heterodimers by celastrol and celastrol-inspired triterpenoids. Oncotarget 6, 32380–32395. 10.18632/oncotarget.6116 . [PubMed: 26474287]
53. Zirath H, Frenzel A, Oliynyk G, Segerström L, Westermark UK, Larsson K, Munksgaard Persson M, Hultenby K, Lehtiö J, Einvik C, et al. (2013). MYC inhibition induces metabolic changes leading to accumulation of lipid droplets in tumor cells. Proc. Natl. Acad. Sci. USA 110, 10258–10263. 10.1073/pnas.1222404110. [PubMed: 23733953]
54. Shachaf CM, Kopelman AM, Arvanitis C, Karlsson A, Beer S,Mandl S, Bachmann MH, Borowsky AD, Ruebner B, Cardiff RD, et al. (2004). MYC inactivation uncovers pluripotent differentiation and tumour dormancy in hepatocellular cancer. Nature 431, 1112–1117. 10.1038/nature03043. [PubMed: 15475948]
55. Zhang W, Meyfeldt J, Wang H, Kulkarni S, Lu J, Mandel JA, Marburger B, Liu Y, Gorka JE, Ranganathan S, and Prochownik EV (2019). beta-Catenin mutations as determinants of hepatoblastoma phenotypes in mice. J. Biol. Chem 294, 17524–17542. 10.1074/jbc.RA119.009979. [PubMed: 31597698]
56. Bratic A, and Larsson NG (2013). The role of mitochondria in aging. J. Clin. Invest 123, 951–957. 10.1172/JCI64125. [PubMed: 23454757]
57. Jang JY, Blum A, Liu J, and Finkel T. (2018). The role of mitochondriain aging. J. Clin. Invest 128, 3662–3670. 10.1172/JCI120842. [PubMed: 30059016]
58. Kauppila TES, Kauppila JHK, and Larsson NG (2017). Mammalian mitochondria and aging: an update. Cell Metabol. 25, 57–71. 10.1016/j.cmet.2016.09.017.
59. Lenaz G, Bovina C, Castelluccio C, Fato R, Formiggini G, Genova ML, Marchetti M, Pich MM, Pallotti F, Parenti Castelli G, and Biagini G. (1997). Mitochondrial complex I defects in aging. Mol. Cell. Biochem 174, 329–333. [PubMed: 9309707]
60. Lesnefsky EJ, Chen Q, and Hoppel CL (2016). Mitochondrial metabolism in aging heart. Circ. Res 118, 1593–1611. 10.1161/CIRCRESAHA.116.307505. [PubMed: 27174952]
61. Srivastava S. (2017). The mitochondrial basis of aging and age-related disorders. Genes 8, 398. 10.3390/genes8120398. [PubMed: 29257072]
62. Pessayre D, Berson A, Fromenty B, and Mansouri A. (2001). Mitochondria in steatohepatitis. Semin. Liver Dis 21, 57–69. 10.1055/s-2001-12929 . [PubMed: 11296697]
63. Rosca MG, Vazquez EJ, Chen Q, Kerner J, Kern TS, and Hoppel CL (2012). Oxidation of fatty acids is the source of increased mitochondrial reactive oxygen species production in kidney cortical tubules in early diabetes. Diabetes 61, 2074–2083. 10.2337/db11-1437. [PubMed: 22586586]
64. Trifunovic A, and Larsson NG (2008). Mitochondrial dysfunction as acause of ageing. J. Intern. Med 263, 167–178. 10.1111/j.1365-2796.2007.01905.x. [PubMed: 18226094]
65. Fazzini F, Lamina C, Raftopoulou A, Koller A, Fuchsberger C, Pattaro C, Del Greco FM, Döttelmayer P, Fendt L, Fritz J, et al. (2021). Association of mitochondrial DNA copy number with metabolic syndrome and type 2 diabetes in 14 176 individuals. J. Intern. Med 290, 190–202. 10.1111/joim.13242. [PubMed: 33453124]
66. Camarda R, Williams J, and Goga A. (2017). In vivo reprogramming of cancer metabolism by MYC. Front. Cell Dev. Biol 5, 35. 10.3389/fcell.2017.00035. [PubMed: 28443280]
67. Dang CV (2011). Therapeutic targeting of Myc-reprogrammed cancer cell metabolism. Cold Spring Harbor Symp. Quant. Biol 76, 369–374. 10.1101/sqb.2011.76.011296. [PubMed: 21960526]
68. Dang CV (2012). MYC on the path to cancer. Cell 149, 22–35. 10.1016/j.cell.2012.03.003. [PubMed: 22464321]
69. Edmunds LR, Sharma L, Kang A, Lu J, Vockley J, Basu S, Uppala R, Goetzman ES, Beck ME, Scott D, and Prochownik EV (2015). c-Myc programs fatty acid metabolism and dictates acetyl-CoA abundance and fate. J. Biol. Chem 290, 20100. 10.1074/jbc.A114.580662.

70. Edmunds LR, Sharma L, Wang H, Kang A, d'Souza S, Lu J, McLaughlin M, Dolezal JM, Gao X, Weintraub ST, et al. (2015). c-Myc and AMPK control cellular energy levels by cooperatively regulating mitochondrial structure and function. PLoS One 10, e0134049. 10.1371/journal.pone.0134049.
71. Goetzman ES, and Prochownik EV (2018). The role for myc in coordinating glycolysis, oxidative phosphorylation, glutaminolysis, and fatty acid metabolism in normal and neoplastic tissues. Front. Endocrinol 9, 129. 10.3389/fendo.2018.00129.
72. Graves JA, Wang Y, Sims-Lucas S, Cherok E, Rothermund K,Branca MF, Elster J, Beer-Stolz D, Van Houten B, Vockley J, and Prochownik EV (2012). Mitochondrial structure, function and dynamics are temporally controlled by c-Myc. PLoS One 7, e37699. 10.1371/journal.pone.0037699.
73. Prochownik EV, and Li Y. (2007). The ever expanding role for c-Myc inpromoting genomic instability. Cell Cycle 6, 1024–1029. 10.4161/cc.6.9.4161. [PubMed: 17426456]
74. Vafa O, Wade M, Kern S, Beeche M, Pandita TK, Hampton GM, and Wahl GM (2002). c-Myc can induce DNA damage, increase reactive oxygen species, and mitigate p53 function: a mechanism for oncogene-induced genetic instability. Mol. Cell 9, 1031–1044. 10.1016/s1097-2765(02)00520-8. [PubMed: 12049739]
75. Bruss MD, Khambatta CF, Ruby MA, Aggarwal I, and Hellerstein MK (2010). Calorie restriction increases fatty acid synthesis and whole body fat oxidation rates. Am. J. Physiol. Endocrinol. Metab 298, E108–E116. 10.1152/ajpendo.00524.2009. [PubMed: 19887594]
76. Houtkooper RH, Argmann C, Houten SM, Cantó C, Jeninga EH, Andreux PA, Thomas C, Doenlen R, Schoonjans K, and Auwerx J. (2011). The metabolic footprint of aging in mice. Sci. Rep 1, 134. 10.1038/srep00134. [PubMed: 22355651]
77. Dang CV (2010). Rethinking the Warburg effect with Myc micromanaging glutamine metabolism. Cancer Res. 70, 859–862. 10.1158/0008-5472.CAN-09-3556. [PubMed: 20086171]
78. Osthus RC, Shim H, Kim S, Li Q, Reddy R, Mukherjee M, Xu Y,Wonsey D, Lee LA, and Dang CV (2000). Deregulation of glucose transporter 1 and glycolytic gene expression by c-Myc. J. Biol. Chem 275, 21797–21800. 10.1074/jbc.C000023200. [PubMed: 10823814]
79. Prochownik EV, and Wang H. (2021). The metabolic fates of pyruvatein normal and neoplastic cells. Cells 10. 10.3390/cells10040762.
80. Toth MJ, and Tchernof A. (2000). Lipid metabolism in the elderly. Eur.J. Clin. Nutr 54 (Suppl 3), S121–S125. 10.1038/sj.ejcn.1601033. [PubMed: 11041083]
81. Li F, Wang Y, Zeller KI, Potter JJ, Wonsey DR, O'Donnell KA,Kim JW, Yustein JT, Lee LA, and Dang CV (2005). Myc stimulates nuclearly encoded mitochondrial genes and mitochondrial biogenesis. Mol. Cell Biol 25, 6225–6234. 10.1128/MCB.25.14.6225-6234.2005. [PubMed: 15988031]
82. Houten SM, Violante S, Ventura FV, and Wanders RJA (2016). The biochemistry and physiology of mitochondrial fatty acid beta-oxidation and its genetic disorders. Annu. Rev. Physiol 78, 23–44. 10.1146/annurev-physiol-021115-105045. [PubMed: 26474213]
83. El-Gharbawy A, and Vockley J. (2018). Inborn errors of metabolism with myopathy: defects of fatty acid oxidation and the carnitine shuttle system. Pediatr. Clin 65, 317–335. 10.1016/j.pcl.2017.11.006 .
84. Mihalik SJ, Goodpaster BH, Kelley DE, Chace DH, Vockley J,Toledo FGS, and DeLany JP (2010). Increased levels of plasma acylcarnitines in obesity and type 2 diabetes and identification of a marker of glucolipotoxicity. Obesity 18, 1695–1700. 10.1038/oby.2009.510. [PubMed: 20111019]
85. Gibson KM, Lee CF, and Hoffmann GF (1994). Screening for defects of branched-chain amino acid metabolism. Eur. J. Pediatr 153, S62–S67. 10.1007/BF02138780. [PubMed: 7957389]
86. Wang H, Lu J, Mandel JA, Zhang W, Schwalbe M, Gorka J, Liu Y, Marburger B, Wang J, Ranganathan S, and Prochownik EV (2021). Patient-derived mutant forms of NFE2L2/NRF2 drive aggressive murine hepatoblastomas. Cell. Mol. Gastroenterol. Hepatol 12, 199–228. 10.1016/j.jcmgh.2021.02.004. [PubMed: 33618031]
87. Chadt A, and Al-Hasani H. (2020). Glucose transporters in adipose tissue, liver, and skeletal muscle in metabolic health and disease. Pflugers Arch. 472, 1273–1298. 10.1007/s00424-020-02417-x. [PubMed: 32591906]

88. Kirkinezos IG, and Moraes CT (2001). Reactive oxygen species and mitochondrial diseases. Semin. Cell Dev. Biol 12, 449–457. 10.1006/scdb.2001.0282. [PubMed: 11735379]

89. Tchkonia T, Morbeck DE, Von Zglinicki T, Van Deursen J, Lustgarten J, Scrable H, Khosla S, Jensen MD, and Kirkland JL (2010). Fat tissue, aging, and cellular senescence. Aging Cell 9, 667–684. 10.1111/j.1474-9726.2010.00608.x. [PubMed: 20701600]

90. Bhadra M, Howell P, Dutta S, Heintz C, and Mair WB (2020). Alternative splicing in aging and longevity. Hum. Genet 139, 357–369. 10.1007/s00439-019-02094-6. [PubMed: 31834493]

91. Deschênes M, and Chabot B. (2017). The emerging role of alternative splicing in senescence and aging. Aging Cell 16, 918–933. 10.1111/acel.12646. [PubMed: 28703423]

92. Gonskikh Y, and Polacek N. (2017). Alterations of the translation apparatus during aging and stress response. Mech. Ageing Dev 168, 30–36. 10.1016/j.mad.2017.04.003. [PubMed: 28414025]

93. Knoch J, Kamenisch Y, Kubisch C, and Berneburg M. (2012). Rare hereditary diseases with defects in DNA-repair. Eur. J. Dermatol 22, 443–455. 10.1684/ejd.2012.1654. [PubMed: 22436139]

94. López-Otín C, Blasco MA, Partridge L, Serrano M, and Kroemer G. (2013). The hallmarks of aging. Cell 153, 1194–1217. 10.1016/j.cell.2013.05.039. [PubMed: 23746838]

95. O'Driscoll M. (2012). Diseases associated with defective responses to DNA damage. Cold Spring Harbor Perspect. Biol 4, a012773. 10.1101/cshperspect.a012773.

96. Park Y, and Gerson SL (2005). DNA repair defects in stem cell function and aging. Annu. Rev. Med 56, 495–508. 10.1146/annurev.med.56.082103.104546. [PubMed: 15660524]

97. Turi Z, Lacey M, Mistrik M, and Moudry P. (2019). Impaired ribosomebiogenesis: mechanisms and relevance to cancer and aging. Aging (Albany NY) 11, 2512–2540. 10.18632/aging.101922. [PubMed: 31026227]

98. Donate LE, and Blasco MA (2011). Telomeres in cancer and ageing. Philos. Trans. R. Soc. Lond. B Biol. Sci 366, 76–84. 10.1098/rstb.2010.0291. [PubMed: 21115533]

99. Opresko PL, and Shay JW (2017). Telomere-associated aging disorders. Ageing Res. Rev 33, 52–66. 10.1016/j.arr.2016.05.009. [PubMed: 27215853]

100. Roake CM, and Artandi SE (2020). Regulation of human telomerase in homeostasis and disease. Nat. Rev. Mol. Cell Biol 21, 384–397. 10.1038/s41580-020-0234-z. [PubMed: 32242127]

101. Yan C, Wan R, and Shi Y. (2019). Molecular mechanisms of pre-mRNA splicing through structural biology of the spliceosome. Cold Spring Harbor Perspect. Biol 11, a032409. 10.1101/cshperspect.a032409 .

102. Meshorer E, and Soreq H. (2002). Pre-mRNA splicing modulations in senescence. Aging Cell 1, 10–16. 10.1046/j.1474-9728.2002.00005.x. [PubMed: 12882348]

103. Tabula Muris Consortium (2020). A single-cell transcriptomic atlas characterizes ageing tissues in the mouse. Nature 583, 590–595. 10.1038/s41586-020-2496-1. [PubMed: 32669714]

104. ENCODE Project Consortium (2004). The ENCODE (ENCyclopedia ofDNA elements) project. Science 306, 636–640. 10.1126/science.1105136. [PubMed: 15499007]

105. Keenan AB, Torre D, Lachmann A, Leong AK, Wojciechowicz ML, Utti V, Jagodnik KM, Kropiwnicki E, Wang Z, and Ma'ayan A. (2019). ChEA3: transcription factor enrichment analysis by orthogonal omics integration. Nucleic Acids Res. 47, W212–W224. 10.1093/nar/gkz446 . [PubMed: 31114921]

106. Benanti JA, Wang ML, Myers HE, Robinson KL, Grandori C, and Galloway DA (2007). Epigenetic down-regulation of ARF expression is a selection step in immortalization of human fibroblasts by c-Myc. Mol. Cancer Res 5, 1181–1189. 10.1158/1541-7786.MCR-06-0372. [PubMed: 17982115]

107. Dean R, Kim SS, and Delgado D. (1986). Expression of c-myc onco-gene in human fibroblasts during in vitro senescence. Biochem. Biophys. Res. Commun 135, 105–109. 10.1016/0006-291x(86)90948-4 . [PubMed: 3954759]

108. Smith JR, Venable S, Roberts TW, Metter EJ, Monticone R, andSchneider EL (2002). Relationship between in vivo age and in vitro aging: assessment of 669 cell cultures derived from members of the Baltimore Longitudinal Study of Aging. J. Gerontol. A Biol. Sci. Med. Sci 57, B239–B246. 10.1093/gerona/57.6.b239. [PubMed: 12023260]

109. Cronin-Fenton DP, Damkier P, and Lash TL (2014). Metabolism and transport of tamoxifen in relation to its effectiveness: new perspectives on an ongoing controversy. Future Oncol. 10, 107–122. 10.2217/fon.13.168. [PubMed: 24328412]

110. Bastide P, Darido C, Pannequin J, Kist R, Robine S, Marty-Double C, Bibeau F, Scherer G, Joubert D, Hollande F, et al. (2007). Sox9 regulates cell proliferation and is required for Paneth cell differentiation in the intestinal epithelium. J. Cell Biol 178, 635–648. 10.1083/jcb.200704152. [PubMed: 17698607]

111. Blasco MA (2005). Telomeres and human disease: ageing, cancer and beyond. Nat. Rev. Genet 6, 611–622. 10.1038/nrg1656. [PubMed: 16136653]

112. Kalb R, Neveling K, Nanda I, Schindler D, and Hoehn H. (2006). Fanconi anemia: causes and consequences of genetic instability. Genome Dyn. 1, 218–242. 10.1159/000092510. [PubMed: 18724063]

113. Iwase T, Wang X, Shrimanker TV, Kolonin MG, and Ueno NT(2021). Body composition and breast cancer risk and treatment: mechanisms and impact. Breast Cancer Res. Treat 186, 273–283. 10.1007/s10549-020-06092-5. [PubMed: 33475878]

114. Kang C, LeRoith D, and Gallagher EJ (2018). Diabetes, obesity, and breast cancer. Endocrinology 159, 3801–3812. 10.1210/en.2018-00574. [PubMed: 30215698]

115. Ling S, Brown K, Miksza JK, Howells L, Morrison A, Issa E, Yates T, Khunti K, Davies MJ, and Zaccardi F. (2020). Association of type 2 diabetes with cancer: a meta-analysis with bias analysis for unmeasured confounding in 151 cohorts comprising 32 million people. Diabetes Care 43, 2313–2322. 10.2337/dc20-0204. [PubMed: 32910779]

116. Renehan AG, Tyson M, Egger M, Heller RF, and Zwahlen M(2008). Body-mass index and incidence of cancer: a systematic review and meta-analysis of prospective observational studies. Lancet 371, 569–578. 10.1016/S0140-6736(08)60269-X. [PubMed: 18280327]

117. Billin AN, and Ayer DE (2006). The Mlx network: evidence for a parallelMax-like transcriptional network that regulates energy metabolism. Curr. Top. Microbiol. Immunol 302, 255–278. 10.1007/3-540-32952-8_10. [PubMed: 16620032]

118. Germano G, Lamba S, Rospo G, Barault L, Magrì A, Maione F, Russo M, Crisafulli G, Bartolini A, Lerda G, et al. (2017). Inactivation of DNA repair triggers neoantigen generation and impairs tumour growth. Nature 552, 116–120. 10.1038/nature24673. [PubMed: 29186113]

119. Jiang T, Shi T, Zhang H, Hu J, Song Y, Wei J, Ren S, and Zhou C. (2019). Tumor neoantigens: from basic research to clinical applications. J. Hematol. Oncol 12, 93. 10.1186/s13045-019-0787-5. [PubMed: 31492199]

120. O'Donnell T, Christie EL, Ahuja A, Buros J, Aksoy BA, Bowtell DDL, Snyder A, and Hammerbacher J. (2018). Chemotherapy weakly contributes to predicted neoantigen expression in ovarian cancer. BMC Cancer 18, 87. 10.1186/s12885-017-3825-0. [PubMed: 29357823]

121. Wang R, Dillon CP, Shi LZ, Milasta S, Carter R, Finkelstein D,McCormick LL, Fitzgerald P, Chi H, Munger J, and Green DR (2011). The transcription factor Myc controls metabolic reprogramming upon T lymphocyte activation. Immunity 35, 871–882. 10.1016/j.immuni.2011.09.021. [PubMed: 22195744]

122. Anisimova AS, Alexandrov AI, Makarova NE, Gladyshev VN, and Dmitriev SE (2018). Protein synthesis and quality control in aging. Aging (Albany NY) 10, 4269–4288. 10.18632/aging.101721. [PubMed: 30562164]

123. Hanahan D, and Weinberg RA (2011). Hallmarks of cancer: the next generation. Cell 144, 646–674. 10.1016/j.cell.2011.02.013. [PubMed: 21376230]

124. Molenaars M, Janssens GE, Williams EG, Jongejan A, Lan J, Rabot S, Joly F, Moerland PD, Schomakers BV, Lezzerini M, et al. (2020). A conserved mito-cytosolic translational balance links two longevity pathways. Cell Metabol. 31, 549–563.e7. 10.1016/j.cmet.2020.01.011.

125. Stefanatos R, and Sanz A. (2011). Mitochondrial complex I: a central regulator of the aging process. Cell Cycle 10, 1528–1532. 10.4161/cc.10.10.15496. [PubMed: 21471732]

126. Balaban RS, Nemoto S, and Finkel T. (2005). Mitochondria, oxidants, and aging. Cell 120, 483–495. 10.1016/j.cell.2005.02.001. [PubMed: 15734681]

127. Edgar D, Shabalina I, Camara Y, Wredenberg A, Calvaruso MA, Nijtmans L, Nedergaard J, Cannon B, Larsson NG, and Trifunovic A. (2009). Random point mutations with major effects on

protein-coding genes are the driving force behind premature aging in mtDNA mutator mice. Cell Metabol. 10, 131–138. 10.1016/j.cmet.2009.06.010.

128. Schumacher B, Pothof J, Vijg J, and Hoeijmakers JHJ (2021). The central role of DNA damage in the ageing process. Nature 592, 695–703. 10.1038/s41586-021-03307-7. [PubMed: 33911272]
129. Zhuang D, Mannava S, Grachtchouk V, Tang WH, Patil S, Wawrzyniak JA, Berman AE, Giordano TJ, Prochownik EV, Soengas MS, and Nikiforov MA (2008). C-MYC overexpression is required for continuous suppression of oncogene-induced senescence in melanoma cells. Oncogene 27, 6623–6634. 10.1038/onc.2008.258. [PubMed: 18679422]
130. Solvie D, Baluapuri A, Uhl L, Fleischhauer D, Endres T, Papadopoulos D, Aziba A, Gaballa A, Mikicic I, Isaakova E, et al. (2022). MYC multimers shield stalled replication forks from RNA polymerase. Nature 612, 148–155. 10.1038/s41586-022-05469-4. [PubMed: 36424410]
131. Ghosh A, and Shcherbik N. (2020). Effects of oxidative stress on protein translation: implications for cardiovascular diseases. Int. J. Mol. Sci 21, 2661. 10.3390/ijms21082661. [PubMed: 32290431]
132. Folgueras AR, Freitas-Rodríguez S, Velasco G, and López-Otín C. (2018). Mouse models to disentangle the hallmarks of human aging. Circ. Res 123, 905–924. 10.1161/CIRCRESAHA.118.312204. [PubMed: 30355076]
133. Kõks S, Dogan S, Tuna BG, González-Navarro H, Potter P, and Vandenbroucke RE (2016). Mouse models of ageing and their relevance to disease. Mech. Ageing Dev 160, 41–53. 10.1016/j.mad.2016.10.001. [PubMed: 27717883]
134. Cuthbert AW, Halstead J, Ratcliff R, Colledge WH, and Evans MJ(1995). The genetic advantage hypothesis in cystic fibrosis heterozygotes: a murine study. J. Physiol 482, 449–454. 10.1113/jphysiol.1995.sp020531. [PubMed: 7714835]
135. Destro-Bisol G, D'Aloja E, Spedini G, Scatena R, Giardina B, and Pascali V. (1999). Brief communication: resistance to Falciparum malaria in alpha-thalassemia, oxidative stress, and hemoglobin oxidation. Am. J. Phys. Anthropol 109, 269–273. 10.1002/(SICI)1096-8644(199906)109:2<269::AID-AJPA11>3.0.CO;2-#. [PubMed: 10378464]
136. Jones TR (1997). Quantitative aspects of the relationship between the sickle-cell gene and malaria. Parasitol. Today 13, 107–111. 10.1016/s0169-4758(96)10083-1. [PubMed: 15275114]
137. Hedrick PW (2012). What is the evidence for heterozygote advantage selection? Trends Ecol. Evol 27, 698–704. 10.1016/j.tree.2012.08.012. [PubMed: 22975220]
138. Grisanzio C, and Freedman ML (2010). Chromosome 8q24-associated cancers and MYC. Genes Cancer 1, 555–559. 10.1177/1947601910381380. [PubMed: 21779458]
139. Matthews SM, Eshelman MA, Berg AS, Koltun WA, and Yochum GS (2019). The Crohn's disease associated SNP rs6651252 impacts MYC gene expression in human colonic epithelial cells. PLoS One 14, e0212850. 10.1371/journal.pone.0212850.
140. Beaulieu ME, Jauset T, Massó -Vallé s D, Martínez-Martín S, Rahl P, Maltais L, Zacarias-Fluck MF, Casacuberta-Serra S, Serrano Del Pozo E, Fiore C, et al. (2019). Intrinsic cell-penetrating activity propels Omomyc from proof of concept to viable anti-MYC therapy. Sci. Transl. Med 11, eaar5012. 10.1126/scitranslmed.aar5012 .
141. Han H, Jain AD, Truica MI, Izquierdo-Ferrer J, Anker JF, Lysy B,Sagar V, Luan Y, Chalmers ZR, Unno K, et al. (2019). Small-Molecule MYC inhibitors suppress tumor growth and enhance immunotherapy. Cancer Cell 36, 483–497.e15. 10.1016/j.ccell.2019.10.001. [PubMed: 31679823]
142. Wang H, Chauhan J, Hu A, Pendleton K, Yap JL, Sabato PE, Jones JW, Perri M, Yu J, Cione E, et al. (2013). Disruption of Myc-Max heterodimerization with improved cell-penetrating analogs of the small molecule 10074-G5. Oncotarget 4, 936–947. 10.18632/oncotarget.1108. [PubMed: 23801058]
143. Prochownik EV, and Vogt PK (2010). Therapeutic targeting of myc. Genes Cancer 1, 650–659. 10.1177/1947601910377494. [PubMed: 21132100]
144. Ness KK, Kirkland JL, Gramatges MM, Wang Z, Kundu M,McCastlain K, Li-Harms X, Zhang J, Tchkonia T, Pluijm SMF, and Armstrong GT (2018). Premature physiologic aging as a paradigm for understanding increased risk of adverse health across the lifespan of survivors of childhood cancer. J. Clin. Oncol 36, 2206–2215. 10.1200/JCO.2017.76.7467. [PubMed: 29874132]

145. Mina AI, LeClair RA, LeClair KB, Cohen DE, Lantier L, and Banks AS (2018). CalR: a web-based analysis tool for indirect calorimetry experiments. Cell Metabol. 28, 656–666.e1. 10.1016/j.cmet.2018.06.019.

146. Chen EY, Tan CM, Kou Y, Duan Q, Wang Z, Meirelles GV, Clark NR, and Ma'ayan A. (2013). Enrichr: interactive and collaborative HTML5 gene list enrichment analysis tool. BMC Bioinf. 14, 128. 10.1186/1471-2105-14-128.

147. Kuleshov MV, Jones MR, Rouillard AD, Fernandez NF, Duan Q, Wang Z, Koplev S, Jenkins SL, Jagodnik KM, Lachmann A, et al. (2016). Enrichr: a comprehensive gene set enrichment analysis web server 2016 update. Nucleic Acids Res. 44, W90–W97. 10.1093/nar/gkw377. [PubMed: 27141961]

148. Xie Z, Bailey A, Kuleshov MV, Clarke DJB, Evangelista JE, Jenkins SL, Lachmann A, Wojciechowicz ML, Kropiwnicki E, Jagodnik KM, et al. (2021). Gene set knowledge discovery with Enrichr. Curr. Protoc 1, e90. 10.1002/cpz1.90. [PubMed: 33780170]

149. Wu T, Hu E, Xu S, Chen M, Guo P, Dai Z, Feng T, Zhou L, Tang W, Zhan L, et al. (2021). ClusterProfiler 4.0: a universal enrichment tool for interpreting omics data. Innovation 2, 100141. 10.1016/j.xinn.2021.100141.

150. Yu G, Wang LG, Han Y, and He QY (2012). clusterProfiler: an R package for comparing biological themes among gene clusters. OMICS 16, 284–287. 10.1089/omi.2011.0118. [PubMed: 22455463]

151. Dobin A, Davis CA, Schlesinger F, Drenkow J, Zaleski C, Jha S,Batut P, Chaisson M, and Gingeras TR (2013). STAR: ultrafast universal RNA-seq aligner. Bioinformatics 29, 15–21. 10.1093/bioinformatics/bts635. [PubMed: 23104886]

152. Ewels PA, Peltzer A, Fillinger S, Patel H, Alneberg J, Wilm A, Garcia MU, Di Tommaso P, and Nahnsen S. (2020). The nf-core frame-work for community-curated bioinformatics pipelines. Nat. Biotechnol 38, 276–278. 10.1038/s41587-020-0439-x. [PubMed: 32055031]

153. Gu Z, Eils R, and Schlesner M. (2016). Complex heatmaps reveal patterns and correlations in multidimensional genomic data. Bioinformatics 32, 2847–2849. 10.1093/bioinformatics/btw313. [PubMed: 27207943]

154. Edgar R, Domrachev M, and Lash AE (2002). Gene Expression Omnibus: NCBI gene expression and hybridization array data repository. Nucleic Acids Res. 30, 207–210. 10.1093/nar/30.1.207. [PubMed: 11752295]

155. Xu J. (2005). Preparation, culture, and immortalization of mouse embryonic fibroblasts. Curr Protoc Mol Biol Chapter 28, mb2801s70, Unit 28 21. 10.1002/0471142727.

156. Castro B, and Kuang S. (2017). Evaluation of muscle performance inmice by treadmill exhaustion test and whole-limb grip strength assay. Bio. Protoc 7, e2237. 10.21769/BioProtoc.2237.

157. Preibisch S, Saalfeld S, and Tomancak P. (2009). Globally optimal stitching of tiled 3D microscopic image acquisitions. Bioinformatics 25, 1463–1465. 10.1093/bioinformatics/btp184. [PubMed: 19346324]

158. Schindelin J, Arganda-Carreras I, Frise E, Kaynig V, Longair M, Pietzsch T, Preibisch S, Rueden C, Saalfeld S, Schmid B, et al. (2012). Fiji: an open-source platform for biological-image analysis. Nat. Methods 9, 676–682. 10.1038/nmeth.2019. [PubMed: 22743772]

159. Schneider CA, Rasband WS, and Eliceiri KW (2012). NIH Image to ImageJ: 25 years of image analysis. Nat. Methods 9, 671–675. 10.1038/nmeth.2089. [PubMed: 22930834]

160. Ruifrok AC, and Johnston DA (2001). Quantification of histochemical staining by color deconvolution. Anal. Quant. Cytol. Histol 23, 291–299. [PubMed: 11531144]

161. Jackson LE, Kulkarni S, Wang H, Lu J, Dolezal JM, Bharathi SS, Ranganathan S, Patel MS, Deshpande R, Alencastro F, et al. (2017). Genetic dissociation of glycolysis and the TCA cycle affects neither normal nor neoplastic proliferation. Cancer Res. 77, 5795–5807. 10.1158/0008-5472.CAN-17-1325. [PubMed: 28883002]

162. Zhang MJ, Pisco AO, Darmanis S, and Zou J. (2021). Mouse aging cell atlas analysis reveals global and cell type-specific aging signatures. Elife 10, e62293. 10.7554/eLife.62293.

163. GTEx Consortium (2013). The genotype-tissue expression (GTEx) project. Nat. Genet 45, 580–585. 10.1038/ng.2653. [PubMed: 23715323]

164. R Core Team (2022). R: A Language and Environment for Statistical Computing. https://www.R-project.org/.

## Highlights

- Postnatal body-wide deletion of the *Myc* gene in mice causes premature aging
- "*Myc*KO" mice dysregulate numerous genes involved in aging, senescence, and cancer
- *Myc*KO mice live longer and have a low lifetime cancer incidence
- Normal aging in mice and humans is associated with *Myc* downregulation

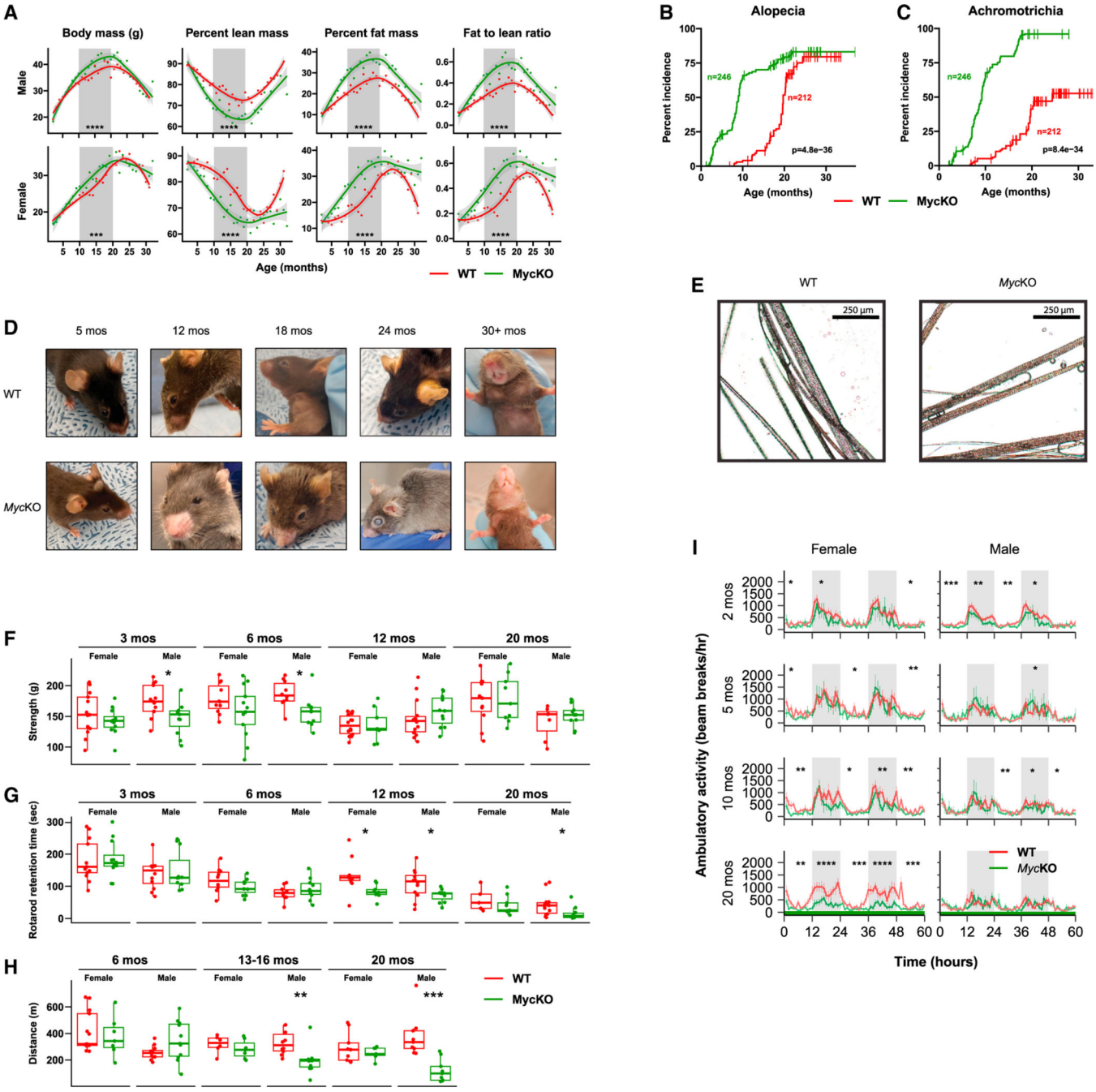


**Figure 1. Young *Myc*KO mice display aging-related phenotypes**

(A) Weight and body composition of male and female WT and *Myc*KO mice. Each point represents the mean of measurements performed on 10–20 animals performed over 2–3 days. Times during which differences existed between the two groups are indicated by gray shading.

(B) Premature alopecia in *Myc*KO mice.

(C) Premature achromotrichia in *Myc*KO mice.

(D) Appearance of representative WT and *Myc*KO mice. See Video S1 for additional examples.
(E) Close-up images of fur from 20-month-old WT and *Myc*KO mice showing the interspersion of dark and gray strands in the former cohort versus the greater uniformity of gray color among individual strands in the latter.
(F) Four-limb GripMeter testing performed on male and female animals. n = 9–13.
(G) Rotarod testing of WT and *Myc*KO mice. n = 5–14.
(H) Treadmill running. Cohorts of WT and *Myc*KO mice were allowed to maintain a continuous pace on an automated treadmill until becoming exhausted. n = 6–13.
(I) Diurnal activity of WT and *Myc*KO mice of the indicated ages as measured in metabolic cages. n = 5–10 males and 5–10 females at each age. White and gray-shaded regions of the plots denote day and night, respectively. (A, F, G, and H) Unpaired t test; (B and C) log rank test; (I) ANOVA[145]; *p < 0.05, **p < 0.01, ***p < 0.001, ****p < 0.0001. Error bars: standard error of the mean (SEM).

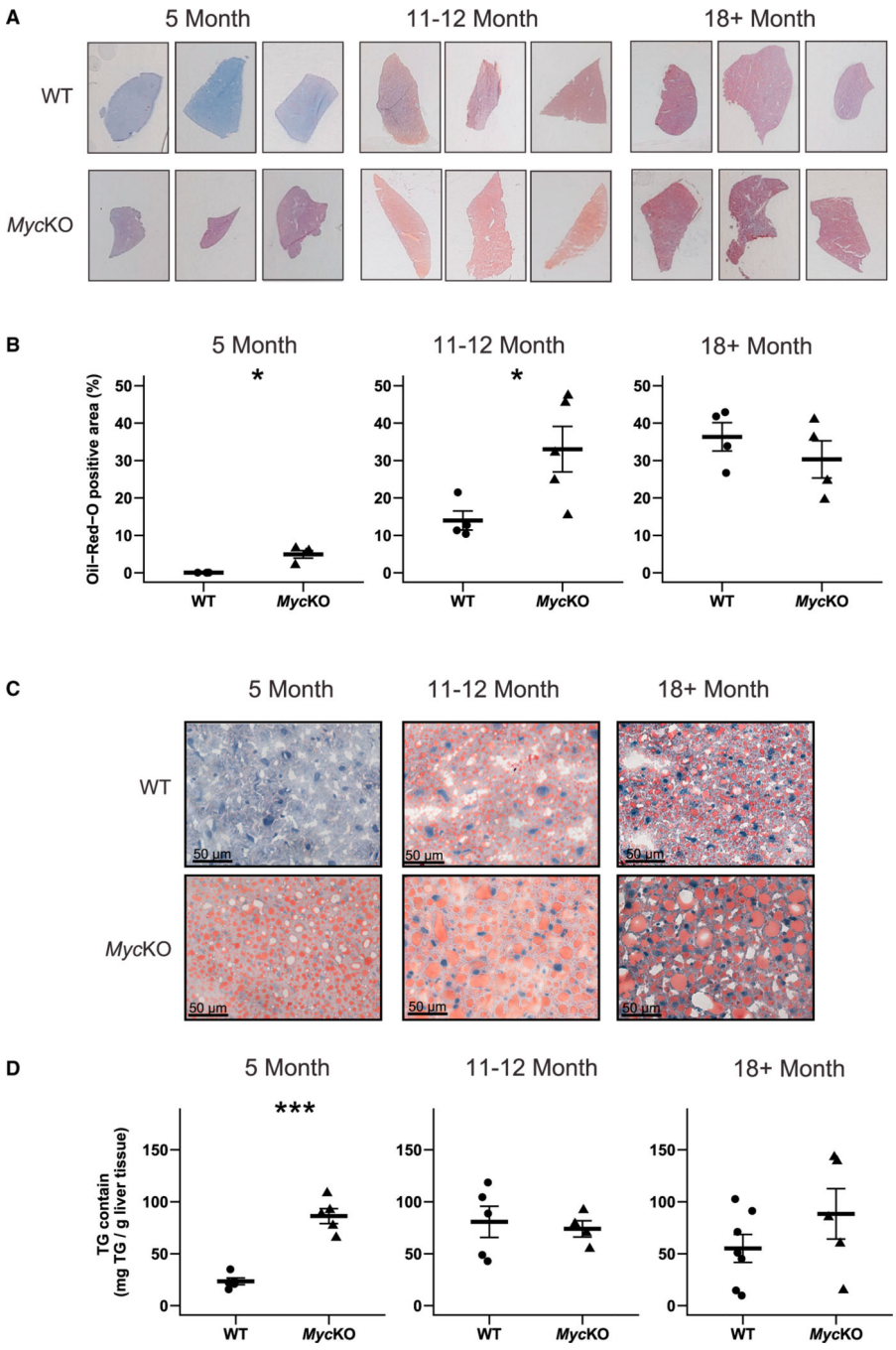


**Figure 2. *Myc*KO mice prematurely develop NAFLD**

(A) Representative oil red O (ORO)-stained liver sections of WT and *Myc*KO mice.

(B) Quantification of ORO-stained sections. At least 3 liver sections from 4 or 5 mice were scanned, quantified, and combined.

(C) Higher-power magnification of the sections from (A) showing a greater prominence of large lipid droplets in *Myc*KO livers.

(D) Triglyceride content of WT and *Myc*KO livers. (B and C) Unpaired t test, *$p < 0.05$, ***$p < 0.001$. Error bars: standard deviation (SD).

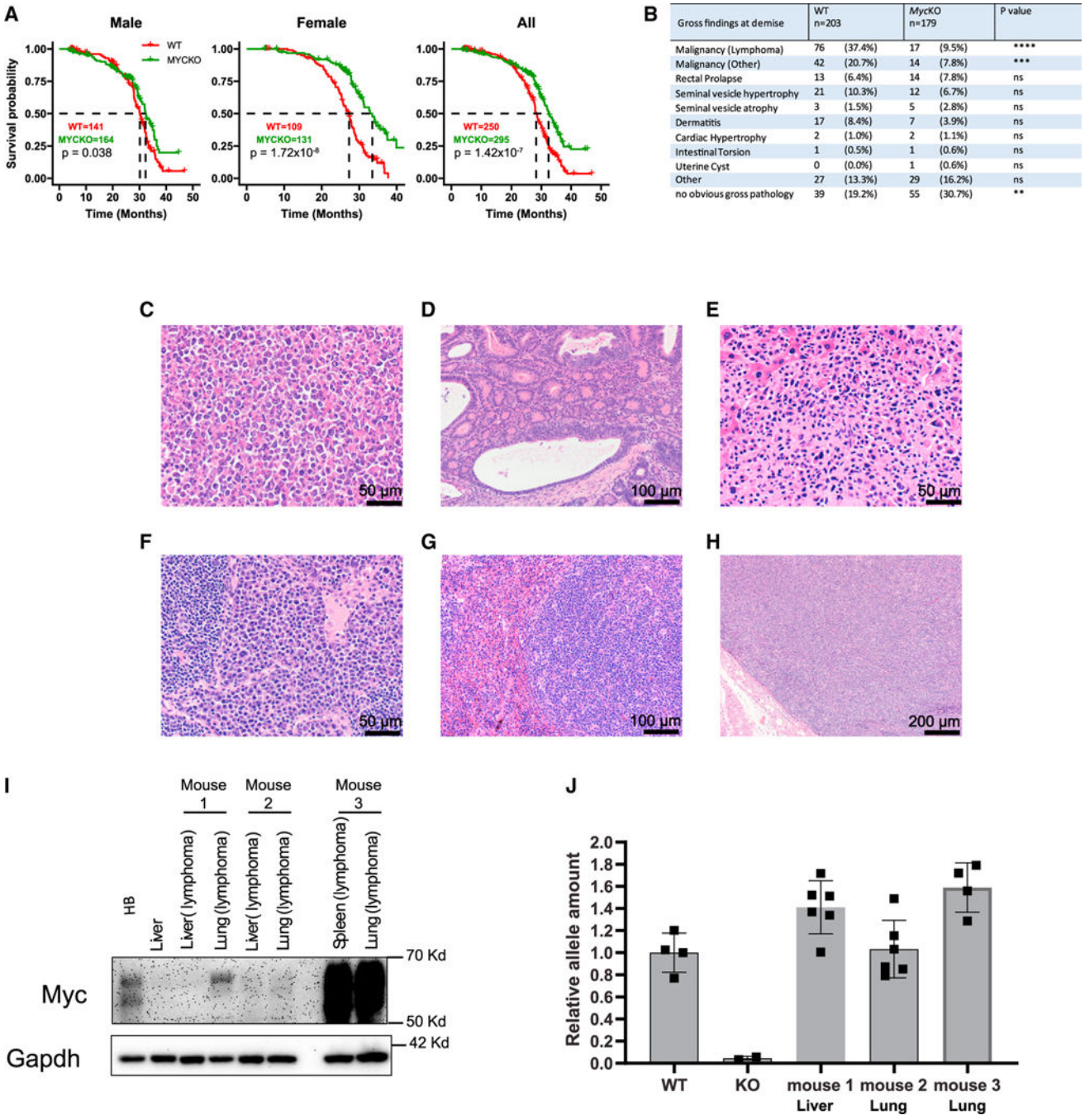


| Gross findings at demise | WT n=203 | | *Myc*KO n=179 | | P value |
|---|---|---|---|---|---|
| Malignancy (Lymphoma) | 76 | (37.4%) | 17 | (9.5%) | **** |
| Malignancy (Other) | 42 | (20.7%) | 14 | (7.8%) | *** |
| Rectal Prolapse | 13 | (6.4%) | 14 | (7.8%) | ns |
| Seminal vesicle hypertrophy | 21 | (10.3%) | 12 | (6.7%) | ns |
| Seminal vesicle atrophy | 3 | (1.5%) | 5 | (2.8%) | ns |
| Dermatitis | 17 | (8.4%) | 7 | (3.9%) | ns |
| Cardiac Hypertrophy | 2 | (1.0%) | 2 | (1.1%) | ns |
| Intestinal Torsion | 1 | (0.5%) | 1 | (0.6%) | ns |
| Uterine Cyst | 0 | (0.0%) | 1 | (0.6%) | ns |
| Other | 27 | (13.3%) | 29 | (16.2%) | ns |
| no obvious gross pathology | 39 | (19.2%) | 55 | (30.7%) | ** |

**Figure 3. *Myc*KO mice have extended lifespans and lower cancer incidence**

(A) Natural lifespans of WT and *Myc*KO male, female, and all mice.

(B) Incidence of associated gross pathologies in WT and *Myc*KO mice at the time of demise.

(C) High-grade lymphoma from a *Myc*KO mouse forming a nodular mass adjacent to a loop of bowel.

(D) Well-differentiated *Myc*KO colonic adenocarcinoma.

(E) High-grade *Myc*KO lymphoma replacing normal liver parenchyma.

(F) Probable *Myc*KO plasmacytoma.
(G) Splenic *Myc*KO lymphoma.
(H) Lymphoma from the mouse in (G) effacing a lymph node adjacent to the pleural surface.
(I) Myc protein expression. Control tissues included normal liver and a hepatoblastoma.[55] Lymphomas from three *Myc*KO mice (#1 to #3) were sampled from the two indicated sites.
(J) *Myc* alleles in *Myc*KO lymphomas (I). *Myc* copy number quantification was performed on several sections of each tumor (Figure S1). DNAs from WT and *Myc*KO primary MEFs (n = 4 each) served as controls for two copies or zero copies, respectively, of an intact *Myc* allele.[23] (A) Log rank test; (B) unpaired t test, **p < 0.01, ***p < 0.001, ****p < 0.0001; ns, not significant; (J) error bars: SD.

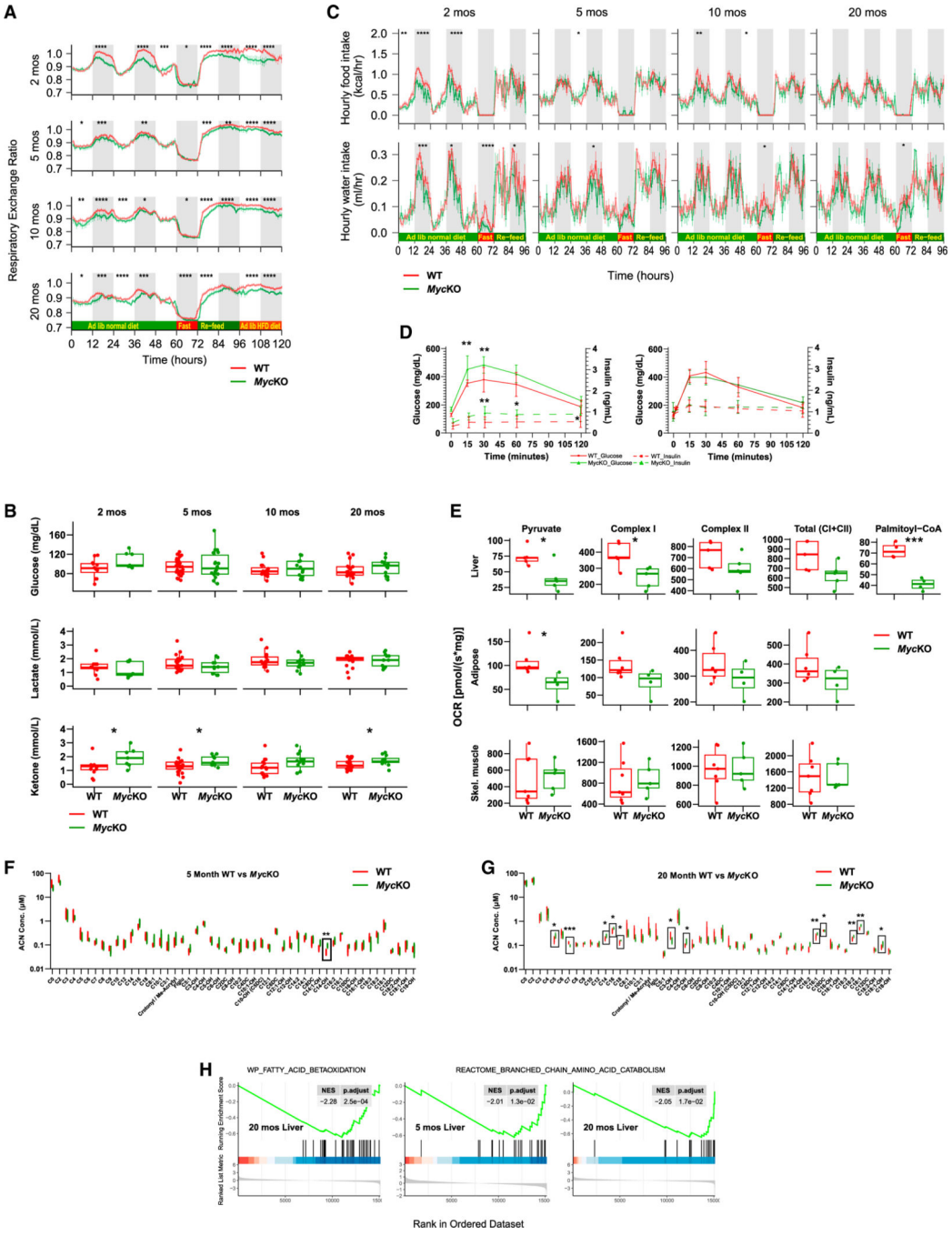


**Figure 4. Metabolic defects in *Myc*KO mice are consistent with premature aging**

(A) Respiratory exchange ratios (RERs) calculated from the formula RER = $VCO_2/VO_2$.[29] At 60 h, mice were fasted for 12 h and then provided with ad *lib* standard (re-feed) or high-fat diets (HFD) for consecutive 24 h periods. Each point is the mean of n = 11–13 mice/group ± 1 SE.

(B) Fasting glucose, lactate, and ketone levels.

(C) Hourly food and water intake (A).

(D) Glucose tolerance tests (GTTs) and serum insulin levels. Mice were fasted for 5 h and then administered a single i.p. bolus of glucose. n = 5.

(E) Oroboros respirometry results performed on mitochondria from the indicated WT and *Myc*KO tissues. Pyruvate responses were determined following the addition of malate and ADP, whereas total complex I activity was determined following the subsequent addition to glutamate.[12,13,23].

(F) Fifty-one serum acyl carnitine levels in 5 month-old WT and KO mice obtained after overnight fasting. n = 5 mice/group. Also see Figures S4 and S5.

(G) The same serum acyl carnitines were assessed in ~20-month-old WT and KO mice as described in (F). n = 5 mice/group. Boxes indicate significant intergroup differences. Also see Figures S4 and S5.

(H) Gene set enrichment analysis (GSEA) for liver transcripts involved in FAO from 20-month-old *Myc*KO mice and additional negative enrichment in 5- and 20-month-old *Myc*KO mice for genes comprising the BCAA catabolic pathway. Results were generated from RNA-seq data obtained from liver, adipose tissue, and skeletal muscle of each of the indicated cohorts, but were significant only in the liver as shown. (A and C) ANOVA,[145] (B, D, E, F, and G) unpaired t test, *$p < 0.05$, **$p < 0.01$, ***$p < 0.001$, ****$p < 0.0001$. Error bars: SD.

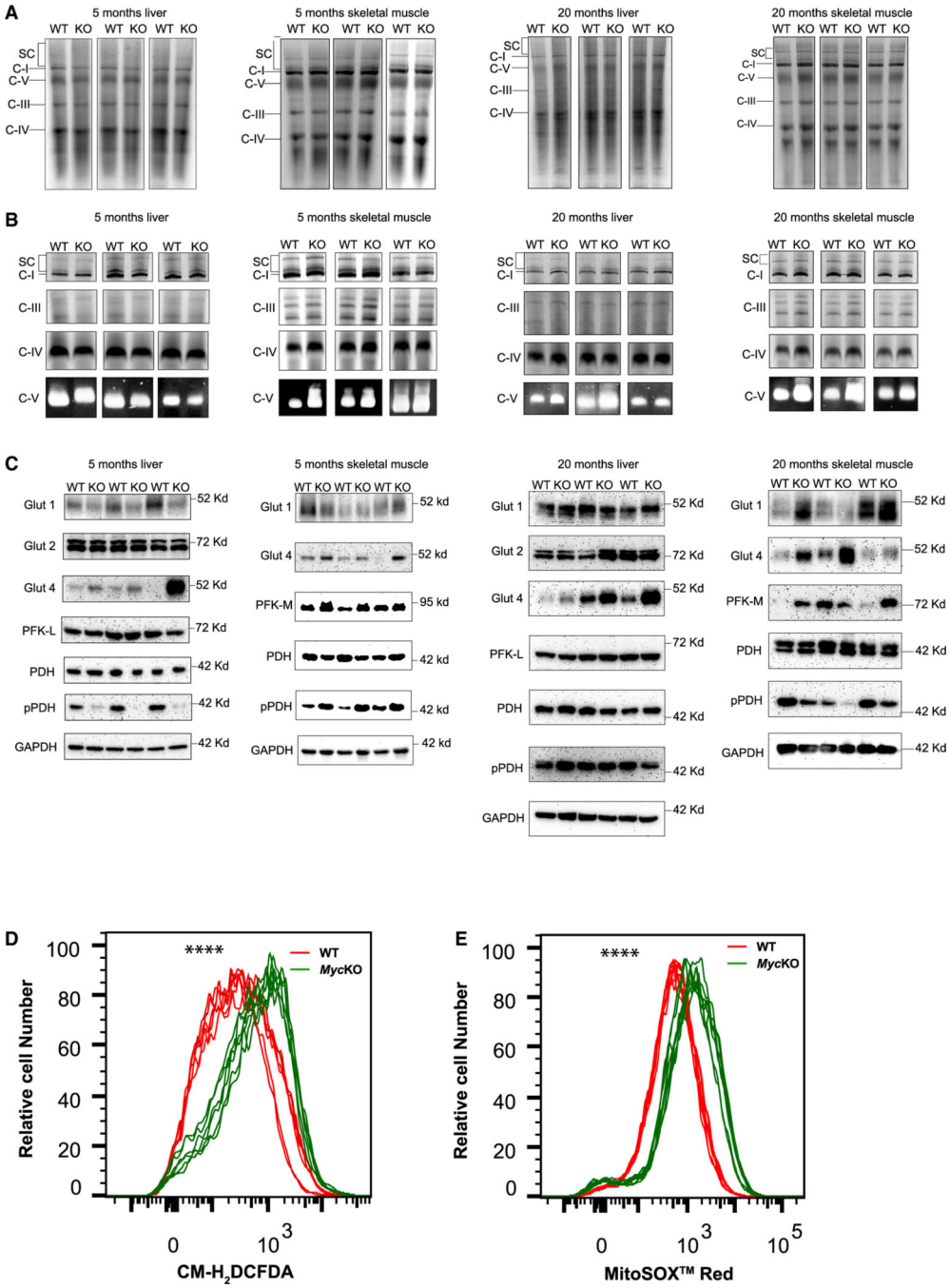


**Figure 5. ETC structure and function and glucose handling differ between WT and *Myc*KO livers and skeletal muscle**

(A) BNGE profiles of liver and skeletal muscle ETC complexes I–IV, complex V, and supercomplexes (SCs) from mitochondria of 5- and 20-month-old mice.[72] SCs comprise higher-order assemblies of complexes I, III, and IV.[72]

(B) *In situ* enzymatic activity of complexes I, III, IV, and V from (A).[72]

(C) Immunoblot analyses of proteins involved in glucose and pyruvate transport and metabolism from the tissues shown in (A) and (B).

(D) ROS production by WT and *Myc*KO MEFs measured by the oxidation of CM-$H^2$DCFDA.[23] n = 6.

(E) Mitochondrial-specific ROS production measured by the superoxide-mediated oxidation of MitoSOX red. n = 6. Unpaired t test, ****$p < 0.0001$.

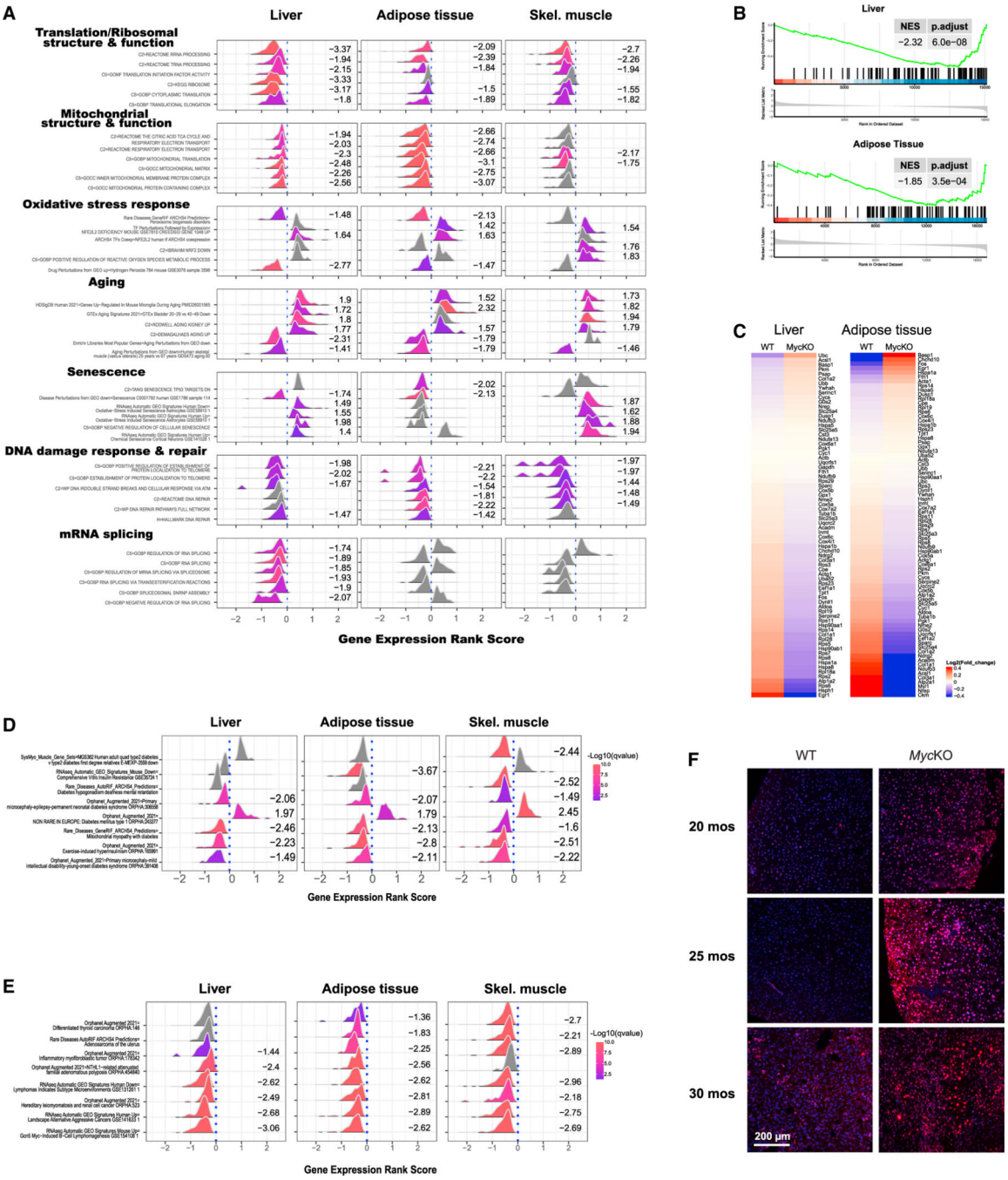


**Figure 6. Tissues from 5-month-old *Myc*KO mice are enriched for aging- and senescence-associated transcripts**

(A) GSEA from tissues of 5-month-old WT and *Myc*KO mice.[146–148] clusterProfiler displays representative examples of the most recurrent and prominent of the gene sets within each category.[149,150] Numbers to the right of each profile indicate its normalized enrichment score. Curves shown in gray and lacking enrichment scores indicate gene sets that were not significantly enriched. Values >0 along the abscissas indicate gene sets that were upregulated in *Myc*KO tissues, whereas values <0 indicate gene sets that were downregulated. See Figure S7 for standard GSEA plots of these.

(B and C) GSEA and heatmap for transcripts that correlate with aging in most tissues and across species in livers and adipose tissue of 5-month-old WT and *Myc*KO mice.
(D) Gene sets associated with types 1 and 2 diabetes selectively enriched in the indicated tissues of 5-month-old *Myc*KO mice.
(E) Gene sets associated with cancer selectively enriched in the indicated tissues of 5-month-old *Myc*KO mice.
(F) Examples of immunostaining for γ-H2AX in the indicated mice depicting double-stranded DNA breaks. Shown are merged micrographs: γ-H2AX immunostaining (red) and DAPI staining (blue).

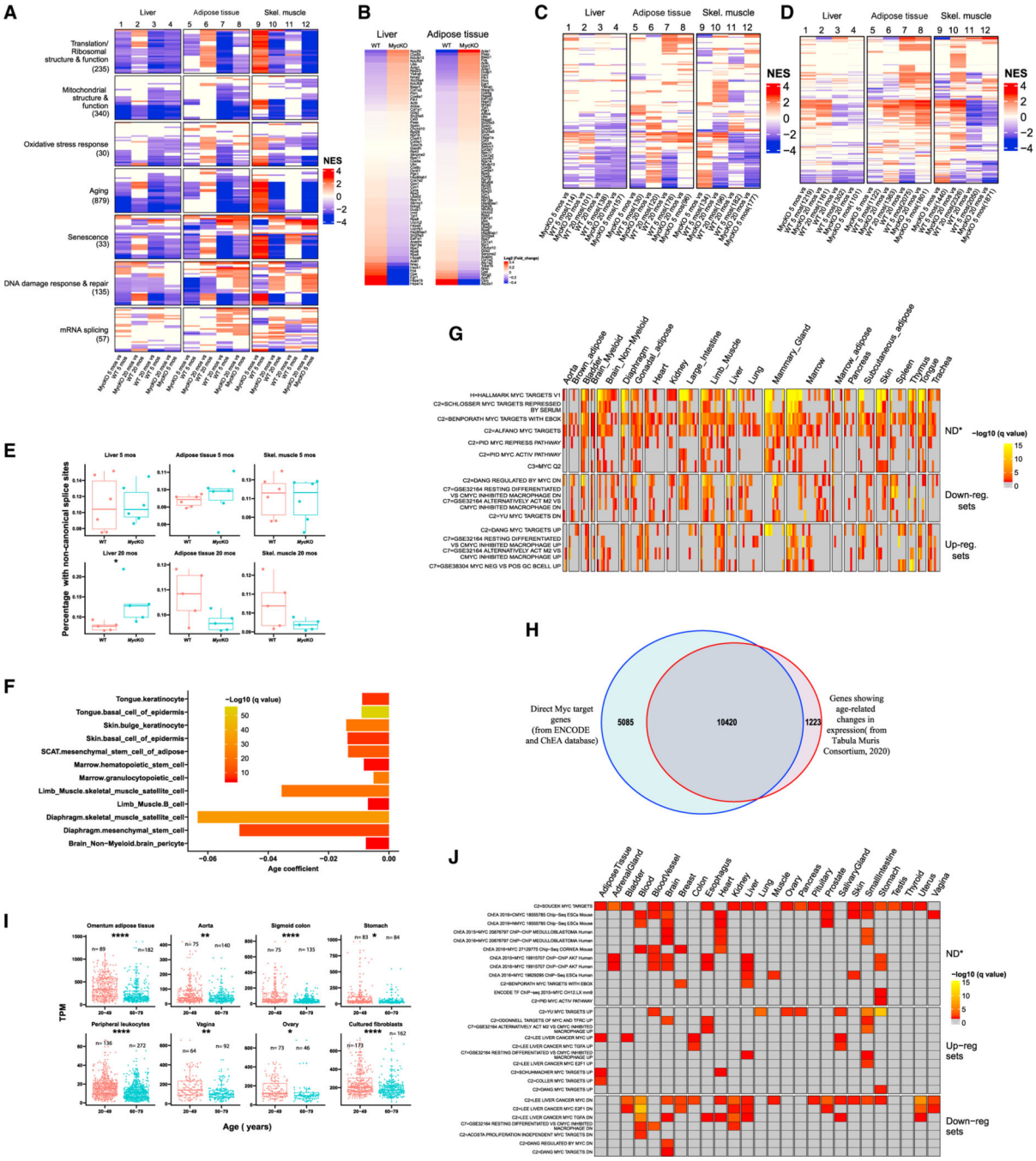


**Figure 7. Gene expression differences in young and old mouse tissues reflect declines in Myc and Myc target genes**

(A) Age- and Myc-dependent gene set enrichment differences among 5- and 20-month-old WT and *Myc*KO tissues. n = 5. The total number of gene sets for which significant enrichment was observed is indicated beneath each category. Colored lines within each category represent a single gene set, the top 30 of which are shown for each category. Data S1 lists all relevant gene sets and others depicted here.

(B) Heatmap for the 79 transcripts shown in Figures 6B and 6C that correlate with aging in most tissues examined and across species.

(C) Heatmap of individual gene sets related to types 1 and 2 diabetes, including those depicted in Figure 6D from 5- and 20-month-old WT and *Myc*KO mice.
(D) Heatmap for the expression of individual gene sets related to cancer, including those depicted in Figure 6E from 5- and 20-month-old WT and *Myc*KO mice.
(E) Transcriptome-wide quantification of non-canonically spliced transcripts.[149–152] Unpaired t test, *$p < 0.05$.
(F) Significant declines in Myc transcript levels in 12 of 90 single-cell populations derived from 23 individual young (1–3 months) and old (18–30 months) mousetissues.[103] Results are expressed as q values based upon correlation coefficients that compared transcript levels across aging populations.
(G) Overrepresentation analysis of 58 Myc target gene sets analyzed using the above-cited single-cell RNA-seq data from young versus old mice.103 Gene sets for which significant dysregulation was observed in at least 40 of the 90 single-cell populations are shown, although 74 of the cell populations (82.2%) showed enriched representation of at least one gene set (Data S1). Down-reg. sets, downregulated in response to Myc overexpression; Up-reg. sets, upregulated in response to Myc overexpression; ND, sets comprising both positive and negative targets whose overall direction of response could not be determined.
(H) Overlap between direct Myc target genes and those that undergo significant age-related changes in expression ($q < 0.05$).[104,105] Gene expression differences were compared from 76 single-cell populations derived from 23 tissues from 1- to 3- and 18- to 30-month-old mice.[103] (I) Myc transcript differences in young and old human tissues. Results are from the Broad Institute's GTEx database.
(J) Enrichment of Myc target gene sets (see Figures S6A–S6C) in aging and senescent human tissues and cell lines. (E and I) Unpaired t test, *$p < 0.05$, **$p < 0.01$, ****$p < 0.0001$.

## KEY RESOURCES TABLE

| REAGENT or RESOURCE | SOURCE | IDENTIFIER |
|---|---|---|
| Antibodies | | |
| Glut 1 | Abcam | Cat#Ab115730; RRID:AB_10903230 |
| Glut 2 | Proteintech | Cat#20436–1-AP; RRID:AB_2750600 |
| Glut 4 | Cell signaling | Cat#2213; RRID:AB_823508 |
| GAPDH | Sigma | Cat#G8795; RRID:AB_1078991 |
| γH2A.X | Abcam | Cat#ab81299; RRID:AB_1640564 |
| PDH | Cell signaling | Cat#3205; RRID:AB_2162926 |
| c-Myc | Cell signaling | Cat#13987; RRID:AB_2631168 |
| c-Myc | Santa Cruz | Cat# sc-764; RRID:AB_631276 |
| p-PDH | Millipore | Cat# AP1062; RRID:AB_10616069 |
| PFK-L | Avivva sys bio | Cat# ARP45774_T100; RRID:AB_1294624 |
| PFK-M | R and D Systems | Cat# MAB7687; RRID:AB_2861389 |
| Rabbit IgG | Cell signaling | Cat# 7074; RRID:AB_2099233 |
| Mouse IgG | Cell signaling | Cat# 7076; RRID:AB_330924 |
| Chemicals, peptides, and recombinant proteins | | |
| ABC-HRP Kit | Vector Laboratories | Cat#PK-6101 |
| 0.25% trypsin-EDTA | Corning | Cat#25–053-CI |
| DMEM | Cytiva | Cat#SH30022.01 |
| Fetal Bovine Serum (FBS) | Biowest | Cat# S1620 |
| 4-hydroxytamoxifen (4-OHT) | Sigma-Aldrich | Cat#H7904 |
| Tamoxifen | Sigma-Aldrich | Cat#T10540–29-1 |
| D-(+)-Glucose solution | Sigma-Aldrich | Cat#G8769 |
| MitoSOX™ Red | Thermo Fisher Scientific | Cat#M36008 |
| CM-$H_2$DCFDA | Thermo Fisher Scientific | Cat#D399 |
| Critical commercial assays | | |
| Ultra Sensitive Mouse Insulin ELISA Kit | Crystal Chem | Cat#90080 |

| REAGENT or RESOURCE | SOURCE | IDENTIFIER |
|---|---|---|
| Senescence Detection Kit | Abcam | Cat#ab65351 |
| Deposited data | | |
| Raw data of RNAseq | This paper | GEO: GSE223676 |
| uncropped western blots deposited at Mendeley Data | This paper | https://doi.org/10.17632/4t9xbmxszn.1 |
| Tabula Muris Consortium mosue single cell RNAseq data | Tabula Muris Consortium | https://figshare.com/ndownloader/files/27856758 |
| RNAseq gene TPMs from young and old human tissues (GTEx Analysis V8 release: RNAseq gene TPMs by tissue) | GTEx | https://gtexportal.org/home/datasets (dbGaP: phs000424.v8.p2) |
| Experimental models: Cell lines | | |
| MEFs | In this paper | Wang et al[23] |
| Experimental models: Organisms/strains | | |
| Mouse: B6.129S6-Myctm2Fwa/Mmjax | JACKSON LABORATORY | Strain # 032046-JAX; RRID:MMRRC_032046-JAX |
| Mouse: B6.129-Gt(ROSA)26Sortm1(cre/ERT2)Tyj/J | JACKSON LABORATORY | Strain # 008463; RRID:IMSR_JAX:008463 |
| Mouse: C57BL/6 | JACKSON LABORATORY | Strain # 000664; RRID:IMSR_JAX:000664 |
| Oligonucleotides | | |
| Primers and probes for qRT-PCR | In this paper | Figure S1D |
| Software and algorithms | | |
| ImageJ- Fiji | NIH | https://fiji.sc/#; RRID:SCR_002285 |
| FlowJo v10 | Becton-Dickinson Biosciences | https://www.flowjo.com/solutions/flowjo/;RRID:SCR_008520 |
| R studio | Posit | https://posit.co/download/rstudio-desktop/; RRID:SCR_000432 |
| GraphPad Prism v9.0 | GraphPad Software Inc. | https://www.graphpad.com;RRID:SCR_002798 |
| Clusterprofiler | Wu et al[149] | https://bioconductor.org/packages/release/bioc/html/clusterProfiler.html; RRID:SCR_016884 |
| ComplexHeatmap | Gu et al[153] | https://bioconductor.org/packages/release/bioc/html/ComplexHeatmap.html; RRID:SCR_017270 |
| ggplot2 | CRAN | https://ggplot2.tidyverse.org/index.html; RRID:SCR_014601 |

| REAGENT or RESOURCE | SOURCE | IDENTIFIER |
|---|---|---|
| survminer | CRAN | https://cran.r-project.org/web/packages/survminer/index.html; RRID:SCR_021094 |
| CLC Genomic Workbench version 21 | QIAGEN | https://digitalinsights.qiagen.com/;RRID:SCR_011853 |
| nf-core/rnaseq-3.4 | Ewels, et al[152] | https://github.com/nf-core/rnaseq |
| Other | | |
| DNeasy Blood & Tissue Kit | QIAGEN | Cat#69504 |
| RNeasy kit | QIAGEN | Cat#74004 |
| QIAzol Lysis Reagent | QIAGEN | Cat#79306 |
| Glucose AimStrip Plus | Germaine Laboratories | Cat#37321 |
| Lactate Plus Analyzer | Sports Resource Group | Model#SN0000101115 |
| Keto-Mojo Ketone Meter | Keto-Check | Model#TD-4279 |
| RNeasy Lipid Tissue Mini Kit | QIAGEN | Cat#74804 |
| SuperScript™ IV First-Strand Synthesis System | Thermo Fisher Scientific | Cat#18091050 |
| 3–12% Native PAGE Novex Bis-Tris gel | Thermo Fisher Scientific | Cat#BN1003BOX |